J. Fluid Mech. (1996), *vol.* 322, *pp.* 165–200

On the wave excitation and the formation of recirculation eddies in an axisymmetric flow of uniformly rotating fluids

By HIDESHI HANAZAKI†
National Institute for Environmental Studies, Tsukuba, Ibaraki 305, Japan

(Received 2 February 1994 and in revised form 12 April 1996)

The inertial waves excited in a uniformly rotating fluid passing through a long circular tube are studied numerically. The waves are excited either by a local deformation of the tube wall or by an obstacle located on the tube axis. When the flow is subcritical, i.e. when the phase and group velocity of the fastest wave mode in their long-wave limit are larger than the incoming axial flow velocity, the excited waves propagate upstream of the excited position. The non-resonant waves have many linear aspects, including the upstream-advancing speed of the wave and the coexisting lee wavelength. When the flow is critical (resonant), i.e. when the long-wave velocity is nearly equal to the axial flow velocity, the large-amplitude waves are resonantly excited. The time development of these waves is described well by the equation derived by Grimshaw & Yi (1993). The integro-differential equation, which describes the strongly nonlinear waves until the axial flow reversal occurs, can predict the onset time and position of the recirculation eddies observed in the solutions of the Navier–Stokes equations. The numerical results and the theory both show that the flow reversal most probably occurs on the tube axis and also when the waves are excited by a contraction of the tube wall. The structure of the recirculation eddies obtained in the solutions of the Navier–Stokes equations at $Re = 10^5$ is similar to the axisymmetric or 'bubble-type' breakdown observed in the experiments of the vortex-breakdown which used a different non-uniform (Burgers-type) rotation. In uniformly rotating fluids the formation of the recirculation eddies has not been observed in the previous numerical studies of vortex breakdown where a straight tube was used and thus the inertial waves were not excited. This shows that the generation of the recirculation eddies in this study is genuinely explained by the topographically excited large-amplitude inertial 'waves' and not by other 'instability' mechanisms. Since the wave cannot be excited in a straight tube even in the non-uniformly rotating flows, the generation mechanism of the recirculation eddies in this study is different from the previous numerical studies for the vortex breakdown. The occurrence of the recirculation eddies depends not only on the Froude number and the strength of the excitation source but also on the Reynolds number since the wave amplitude generally decreases by the viscous effects. Some relations to the experiments of vortex breakdown, which have been exclusively done for non-uniformly rotating fluids but done in a 'non-uniform tube', are discussed. The flow states, which are classified as supercritical, subcritical or critical in hydraulic terminology, changes along the flow when the upstream flow is near resonant conditions and a non-uniform tube is used.

† Also Department of Mechanical Engineering, University of Tokyo, Hongo, Bunkyo-ku, Tokyo 113, Japan.

1. Introduction

The flows of rotating fluids passing through a circular tube have been studied as one of the most fundamental problems in fluid mechanics (see figure 1). Among those the uniformly rotating (solid-body rotation) flow has been studied most extensively (see chapter 7 of Batchelor, 1967). When the azimuthal velocity is very large, a column of fluid, called a Taylor column, is pushed ahead of the obstacle placed on the tube axis (Taylor 1922). This occurs when the Rossby number $Ro = U/\Omega a$, defined by U the uniform axial velocity, Ω the uniform angular velocity and a the obstacle radius, satisfies $Ro \leqslant 0.3$. The phenomenon is essentially explained by the steady Euler equation and has little direct relation to the inertial waves. However, both the Taylor column and the inertial waves are observed in the same rotating fluid system and the only difference is that larger azimuthal velocity is necessary for the onset of the Taylor column compared to the excitation of the lowest-mode inertial wave. In this study, the main concern is in the inertial waves excited without the generation of the Taylor column. This means that the azimuthal velocity is large enough to support the inertial waves but small enough to avoid the generation of the Taylor column.

It is well-known in the linear theory for the steady inertial wave (Batchelor 1967) that standing lee waves are formed downstream of the obstacle if the azimuthal velocity is large enough (cf. figure 2). The theoretical prediction of the wavelength in uniformly rotating fluids has been compared with the experiments by Long (1953) and Pritchard (1968) and good agreement has been obtained. At first sight, the usefulness of the linear theory seems to be clear when the flow is steady and has a uniform rotation, since the exact fully nonlinear governing equations become 'linear' without any linearization processes under the assumption of 'no upstream influence'. However, the unsteady linear theory or the linear dispersion relation predicts that when the steady lee waves are formed, there is always a wave with longer wavelength which propagates upstream of the obstacle, invalidating the assumption of no upstream influence. This also shows that the flow is always subcritical to the excited lee-wave modes (Benjamin 1970; McIntyre 1972; Hanazaki 1989). The problem of upstream influence occurs also when the rotation is non-uniform, e.g. the Burgers-type rotation. In this study we assess this problem by comparing the numerical results with the linear theory.

The solution by the linear theory diverges when the flow is critical (or resonant), i.e. when the phase and the group velocity of the linear wave in the long-wave limit is identical to the incoming axial flow velocity. In this case the wave energy of long-wave components accumulates near the obstacle and cannot propagate away from the obstacle (cf. figure 2*b*). Then the wave amplitude increases in proportion to the elapsed time, leading to the divergence of the linear solution in the long-time limit or in the steady state.

In the general rotating flows the application of weakly nonlinear theories can avoid the divergence and describe the waves near resonant conditions. For the case with no topographic effects, Benjamin (1967) and Leibovich (1969, 1970) showed the possible existence of the solitary waves governed by the Korteweg–de Vries (KdV) equation. Leibovich & Randall (1973) extended it to an equation with a forcing term due to the deformation of the tube wall and solved it for some special initial and boundary conditions (Randall & Leibovich 1973). Grimshaw (1990) derived a similar equation but with a slightly different forcing term. The main difference from Leibovich & Randall's equation was that the slow variation of the forcing in the axial direction was not assumed. The equation derived by Grimshaw (i.e. forced KdV equation) is identical in form to the equation recently derived and studied extensively in the similar

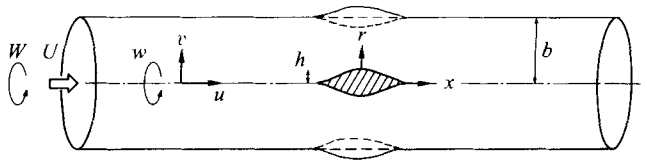

FIGURE 1. Schematical view of the flow geometry.

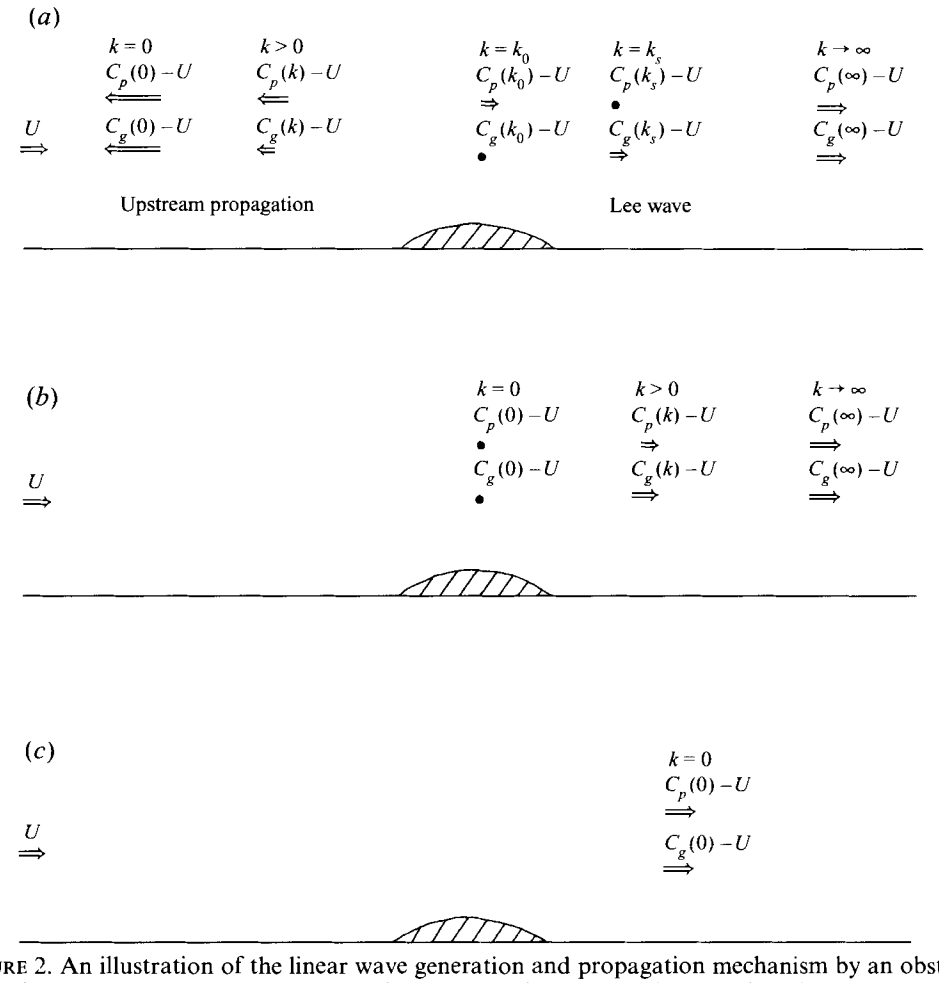

FIGURE 2. An illustration of the linear wave generation and propagation mechanism by an obstacle. These figures assume that $C_p(k) > C_g(k)$ $(k \neq 0)$, $\partial C_p/\partial k < 0$, $\partial C_g/\partial k < 0$ and $C_p(k=0) = C_g(k=0)$ as in the inertial waves in the uniformly rotating fluid. Similar phenomena occur in water waves and internal gravity waves. The three figures show the cases of (*a*) subcritical, (*b*) critical (resonant) and (*c*) supercritical upstream flows, respectively.

contexts of the water waves (Wu 1981; Akylas 1984; Lee, Yates & Wu 1989) and the internal waves in stratified fluids (Grimshaw & Smyth 1986). It is now known that the equation is, in general, applicable to these problems except for the interfacial waves in two-layer fluids, where consideration of the higher-order nonlinearity is usually necessary (Melville & Helfrich 1987; Hanazaki 1992). Therefore we could anticipate that the weakly nonlinear waves excited in rotating flows would be generally described by the forced KdV equation. This has been verified by comparing its solution with the solution of the Navier–Stokes equations near resonant conditions for the Burgers-type

vortex (Hanazaki 1991, 1993*a*). The results agree in the appearance of the periodically generated upstream-advancing solitary waves, downstream flat depressions elongated with time and the further downstream-advancing lee waves.

However, if the swirl has a uniform (i.e. solid-body) rotation, all the coefficients of the nonlinear terms of the KdV-type equations, i.e. AA_X, A^2A_X, vanish irrespective of the existence of the obstacle, and the nonlinearity cannot be described by the KdV-type equations (Grimshaw 1990). In general, this occurs when the fully nonlinear governing equations for steady state become 'linear' without any linearization processes. The same difficulty occurs in the linearly stratified Boussinesq fluid, which has been studied most extensively in the field of stratified flows. However, in that context Grimshaw & Yi (1991) derived a new type of integro-differential equation which describes the strongly nonlinear waves near resonance and Hanazaki (1993*b*) and recently Rottman, Broutman & Grimshaw (1996) compared its solution with the solution of the Navier–Stokes equations and showed that the equation is a quantitatively good approximation to the fully nonlinear equations, even predicting the onset of the flow reversal, i.e. the wave breaking. More recently Grimshaw & Yi (1993) derived the essentially same equation for the waves in a uniformly rotating fluid. The new equation, which hereinafter we call the Grimshaw–Yi (GY) equation, describes the strongly nonlinear waves and can describe large-amplitude waves until the axial flow reversal occurs. Therefore, we can expect that the GY equation predicts the onset of recirculation eddies in the uniformly rotating fluids whose origins are in the large-amplitude inertial waves, although it cannot describe the subsequent time development. Since the recirculation eddies in this study are generated by a large amplitude wave which occurs when the flow is near 'resonant (critical)' conditions, our solutions for the unsteady flow show the 'critical' generation of the eddies.

The main purpose of this paper is the investigation of the fundamental linear and nonlinear aspects of the waves excited in uniformly rotating flows and not the precise reproduction of the vortex breakdown phenomena which have been observed experimentally in rotating flows. However, it would be of interest to discuss how our results relate to those phenomena, since the experiments for the vortex breakdown have been done exclusively in a tube with a 'non-uniform radius' (Harvey 1962; Sarpkaya 1971; Faler & Leibovich 1977, 1978). They have been done sometimes in a tube with a local contraction (Kirkpatrick 1965; or see figure 6 of Hall 1972), which is similar to one of the tubes used in this study. Although the experiments have been done with a non-uniform rotation such as the Burgers-vortex type, if the 'wave' is the essential aspect of the vortex breakdown phenomena, the uniformly rotating flow also should contain the essential mechanisms of the vortex breakdown. The propagation mechanism of the wave is independent of the rotation type and is classified only by the hydraulic terminology, i.e. subcritical, critical and supercritical (cf. figure 2). In analogy with the hydraulic theory, Benjamin (1962, 1967) proposed the existence of the 'critical' state in the steady flow, which separates the supercritical state upstream of the breakdown from the subcritical state downstream of the breakdown. This occurs when the upstream flow is near critical (resonant) condition and the tube radius becomes larger at a certain position so that the axial velocity becomes smaller in the downstream region. The diverging tube was actually used in the experiments by Sarpkaya (1971) and Faler & Leibovich (1977, 1978). The transition between the flow states in the hydraulic sense can be expected also in the flow with a tube deformation used in this study. For example, if there is a local contraction of the tube wall, a critical (resonant) upstream flow becomes slightly supercritical near the contraction and becomes critical again downstream of the contraction.

Numerical studies for the axisymmetric vortex breakdown was first done by Kopecky & Torrance (1973). They solved the steady Navier–Stokes equations with uniform axial velocity and with uniform (solid-body) or non-uniform (Burgers-vortex type) rotation, then reproduced the patterns of the axisymmetric vortex breakdown similar to the experiments only when the non-uniform rotation was used. They noticed that the breakdown occurs always at the upstream boundary of the computed region and the occurrence of the breakdown should affect the upstream boundary condition. They argued that the problem of 'upstream influence' (Benjamin 1970; McIntyre 1972) has to be assessed for our further understanding of the phenomena.

Later numerical simulations for the vortex breakdown all report the recirculation eddies at the upstream boundary of the computed region irrespective of whether the flow is steady (e.g. Grabowski & Berger 1976; Beran 1987; Hafez *et al.* 1986, 1987; Salas & Kuruvila 1989) or unsteady (Menne 1988). To avoid this problem, Beran & Culick (1992) used a local contraction of the tube wall near the upstream boundary in their solutions of the steady Navier–Stokes equations, so that the breakdown occurs always downstream of the contraction. In a recent review paper, Leibovich (1991) showed a serious concern about the previous numerical studies in which the breakdown occurred always at the upstream boundary of the tube, violating the upstream boundary conditions.

It is important to note that Kopecky & Torrance (1973, p. 291) did not observe the vortex breakdown in the case of the uniform rotation even when they changed substantially the upstream axial and swirl velocity. This shows that the vortex breakdown does not occur in a straight tube when the flow has a uniform rotation. Since the inertial waves cannot be excited in a straight tube irrespective of the rotation type, their results suggests that the vortex breakdowns observed in the non-uniform rotations in previous numerical simulations do not have their origin in the waves, although the generated disturbances by some other mechanisms, such as the instabilities, might be advected by the waves. Leibovich (1991) argued also the possibility of the upstream propagation of the disturbances generated at the downstream end of the computed region when the flow is subcritical, although this was not observed in this study in which a very long tube was used.

In this study we consider the inertial waves in a uniformly rotating fluid excited by the deformed tube or an obstacle. We consider the subcritical, critical (resonant) and supercritical upstream flows whose classifications depend on the ratio of the azimuthal flow velocity to the axial flow velocity. In the case of subcritical flows the problem of 'upstream influence' is investigated here as a phenomenon of the wave propagation. When the flow is near resonance and the wave amplitude becomes large, the axial flow reversal or the generation of recirculation eddies occur. The generation mechanism of the recirculation eddies is in the 'waves' excited by the boundary deformation and would be different from the previous numerical studies of the vortex breakdown. This does not mean that our results have no relation to the experiments of the vortex breakdown if the essential aspects are in the 'non-uniform tube' or the 'waves' and not in the non-uniform rotation. The investigation of the applicability of the Grimshaw–Yi equation near resonant conditions is important since it can describe the large-amplitude waves leading to the axial flow reversal and the recirculation eddies. We should note that in the previous numerical studies of the vortex breakdown, direct comparisons with the theories have not been done so that the mechanisms of the breakdown have remained largely unknown. This study is a test of one mechanism, i.e. the generation of the recirculation eddies by the large-amplitude 'inertial waves' excited near the critical (resonant) conditions in the hydraulic sense.

In §2 we review the linear theory and the GY equation. In §§3 we describe the numerical method. In §§4 and 5, the results and the conclusions are given.

2. Review of the theory

We consider the inertial waves excited either by an obstacle on the tube axis or by a local deformation of the tube wall (figure 1). Throughout this paper, we consider the flow with a uniform axial velocity and a uniform (solid-body) rotation at the inflow boundary. In this section we first review the linear theory and then review and discuss the important aspects of the Grimshaw–Yi equation.

First, we describe the governing equations. All the quantities hereinafter are non-dimensionalized by the tube radius b, and the uniform axial velocity at the inflow boundary U, unless otherwise stated. Then using the Reynolds number defined by $Re = Ub/\nu$ (ν = the kinematic viscosity coefficient), the governing equations for the unsteady axisymmetric flow of incompressible fluid (figure 1) are written in cylindrical coordinates as

$$\frac{\partial u}{\partial t}+u\frac{\partial u}{\partial x}+v\frac{\partial u}{\partial r}=-\frac{\partial p}{\partial x}+\frac{1}{Re}\nabla^2 u, \tag{1a}$$

$$\frac{\partial v}{\partial t}+u\frac{\partial v}{\partial x}+v\frac{\partial v}{\partial r}-\frac{w^2}{r}=-\frac{\partial p}{\partial r}+\frac{1}{Re}\left(\nabla^2 v-\frac{v}{r^2}\right), \tag{1b}$$

$$\frac{\partial w}{\partial t}+u\frac{\partial w}{\partial x}+v\frac{\partial w}{\partial r}+\frac{vw}{r}=\frac{1}{Re}\left(\nabla^2 w-\frac{w}{r^2}\right), \tag{1c}$$

$$\frac{\partial u}{\partial x}+\frac{1}{r}\frac{\partial (rv)}{\partial r}=0, \tag{1d}$$

where u, v and w are the axial, radial and azimuthal velocities of the fluid, p is the pressure and ∇^2 is defined by

$$\nabla^2=\frac{\partial^2}{\partial x^2}+\frac{\partial^2}{\partial r^2}+\frac{1}{r}\frac{\partial}{\partial r}. \tag{1e}$$

The momentum equation for the azimuthal velocity (1c) can be rewritten as an equation for the circulation $\Gamma(=rw)$:

$$\frac{\mathrm{D}(rw)}{\mathrm{D}t}=\frac{1}{Re}\left[\nabla^2(rw)-\frac{2}{r}\frac{\partial (rw)}{\partial r}\right], \tag{2a}$$

with

$$\frac{\mathrm{D}}{\mathrm{D}t}=\frac{\partial}{\partial t}+u\frac{\partial}{\partial x}+v\frac{\partial}{\partial r}. \tag{2b}$$

This represents the piecewise conservation of the circulation Γ if there is no viscosity ($Re=\infty$) or if the condition

$$\nabla^2(rw)-\frac{2}{r}\frac{\partial (rw)}{\partial r}=0, \tag{2c}$$

is satisfied.

In the incompressible stratified flows, density is conserved if there is no diffusivity of density and we can consider the circulation Γ as the counterpart of it. It should be noted that (2c) holds when the flow has a uniform (solid-body) rotation, i.e. when the azimuthal velocity is given by $w=r\Omega$, where Ω (= const) is a uniform angular velocity.

Note that $\nabla^2 w - w/r^2$ in the right-hand side of (1*c*) also vanishes in this case. These facts show that the effects of the viscosity in the azimuthal direction becomes ineffective if the flow has a uniform rotation. The circulation is then piecewise conserved even when there is a viscosity of the fluid. If in addition the flow is steady, the contours of the circulation coincide with the Stokes streamlines.

In this study the rotation is approximately uniform except where the large-amplitude waves appear and at the same time the Reynolds number is generally large ($Re = 10^4$). In addition the time development of the flow is generally slow except the inside of the recirculation eddies. Therefore we can use the difference between the contours of circulation and the streamlines as a measure of the unsteadiness and the non-uniformness of the rotation in the recirculation region.

2.1. *Linear theory*

We first review the linear theory. To clarify the physical meanings of the expressions, dimensional quantities are used only in this subsection (§2.1). When the flow has a uniform rotation, the stream function $\psi(x, r, t)$ can be written as (Batchelor 1967)

$$\psi = \tfrac{1}{2}Ur^2 + Bf(r)\sin[k(x + C_p t)], \tag{3a}$$

where B is an arbitrary constant, C_p is the axial phase velocity of the inertial wave and k is the axial wavenumber. The function $f(r)$ is given by

$$f(r) = rJ_1\left\{\left(\frac{4\Omega^2}{C_p^2} - k^2\right)^{1/2} r\right\}, \tag{3b}$$

where J_1 is the Bessel function of the first kind of order one.

Since $f(r)$ satisfies $f(b) = 0$, the phase velocity C_p has to satisfy

$$C_p = \frac{2b\Omega}{(j_n^2 + b^2k^2)^{1/2}}. \tag{4}$$

where j_n ($n = 1, 2, \ldots$) are the nth zeros of $J_1(r)$. This determines the linear dispersion relation $\omega = C_p k$, then the group velocity C_g ($= \partial\omega/\partial k$) becomes

$$C_g = C_p \frac{j_n^2}{j_n^2 + b^2k^2}, \tag{5}$$

showing that $C_p > C_g$ holds always when $k \neq 0$.

The expressions (4) and (5) show that both C_p and C_g become maximum in the long-wave limit ($k = 0$), giving

$$C_n \equiv C_p(k = 0) = C_g(k = 0) = \frac{2b\Omega}{j_n}. \tag{6}$$

Since this value becomes smaller with the increase of n, the fastest wave is the mode $n = 1$ wave of infinite wavelength ($k = 0$) whose velocity is $C_1 = 2b\Omega/j_1$. If $C_1 > U$, this fastest wave propagates upstream of its excited position at a speed of $C_1 - U$ (see figure 2*a*). For the criterion of the appearance of the upstream advancing wave, we use here the Froude number F determined by

$$F = \frac{U}{C_1}. \tag{7}$$

Then if $F < 1$, the flow is subcritical to the mode $n = 1$ and there is an upstream

propagation of the linear wave, while if $F > 1$, the flow is supercritical to all the modes and no upstream propagation occurs. If $F = 1$, the flow is resonant since the long-wave components of the mode 1 wave cannot propagate away from the excited position and the wave energy accumulates there proportional to time (figure 2*b*). Then the linear time-dependent solution or the solution for the steady state diverges. For this case the amplitude becomes large anyway and we have to consider nonlinear effects. More generally, if $C_n = U$ the flow is resonant to mode n and this resonant mode would have the largest amplitude. As is well known in the contexts of the water waves or the internal gravity waves, the standing wave such as the ship wave or the mountain lee wave has the wavenumber k_s which satisfies $C_p(k_s) = U$, which means that the phase of the wave does not move against the topography. Since $C_p > C_g$ and thus $U = C_p(k_s) > C_g(k_s)$ holds for most of the familiar wave systems, the wave energy of the lee waves is swept downstream, exemplifying that standing waves always appear downstream of the excited position (cf. figure 2*a*). In the case of the uniformly rotating flow, the wavelength λ_s ($= 2\pi/k_s$) is given by

$$\lambda_s = \frac{2\pi b}{j_n\left(\frac{C_n^2}{U^2}-1\right)^{1/2}}. \tag{8}$$

It is important here to note that

$$C_p(k=0) = C_g(k=0) > C_p(k_s). \tag{9}$$

This shows that, when there is a standing wave ($C_p(k_s) = U$), the long waves ($k = 0$) of the same mode always propagate upstream. In other words, lee waves and the upstream advancing waves of the same mode n must always coexist.

If the Froude number F is near 1 (but $F < 1$), only the mode $n = 1$ components propagate upstream and only the mode $n = 1$ lee waves exist. The criterion for the generation of the upstream and downstream waves, i.e. $C_1 > U$, can be rewritten as $U/b\Omega < 2/j_1 = 0.522$ and we note that even if $U/b\Omega = 0.522$, the Rossby number Ro satisfies $Ro = U/a\Omega > 0.522 > 0.3$ because the radius of the obstacle must be smaller than the tube radius ($a < b$). This shows that there must be a state with the upstream and the downstream waves but without the generation of the Taylor column. In this study we consider only this case as noted in the introduction.

2.2. *Grimshaw–Yi (GY) equation*

Near resonant conditions ($C_n = U$) the solutions by the linear theory diverge and we have to develop the nonlinear theories which will treat the resonant growth of the inertial wave. If the rotation is non-uniform as in the Burgers-vortex type rotation, we can derive the KdV-type equations (e.g. the forced KdV equation; Grimshaw 1990). However, an important point to note here is that all the coefficients of the nonlinear terms in the KdV-type equations (i.e. the coefficients of AA_X, A^2A_X) vanish when the rotation is uniform (solid-body rotation). In general, this occurs when the inviscid and steady form of the original fully nonlinear governing equations becomes linear without any linearization processes (Appendix to Grimshaw 1990). Grimshaw & Yi (1993) derived a new type of integro-differential equation which describes the nonlinearity of the waves in this particular but typical and important case. For the derivation of the GY equation, we assume that the resonant nth mode is dominant and decompose the stream function as

$$\psi = \tfrac{1}{2}r^2 + A_n(X,T)f_n(r) + \epsilon\psi_1 + O(\epsilon^2), \tag{10a}$$

where
$$f_n(r) = rJ_1(j_n r), \tag{10b}$$
is identical to (3*b*). The second term on the right-hand side of (10*a*) denotes the $O(1)$ (strongly nonlinear) correction to the undisturbed uniform axial velocity and the GY equation describes the time-development of $A_n(X, T)$. In the derivation of the GY equation, the scalings of the axial coordinates and the time are the same as in the derivation of the forced KdV equation, i.e.
$$X = \epsilon^{1/2}x, \quad T = \epsilon^{3/2}t, \tag{11}$$
where $\epsilon = (b/L)^2$ is the square of the ratio of the tube radius to the typical axial wavelength L. The scaling for the amplitude of the boundary deformation is different from the forced KdV equation. It is given by
$$r = \epsilon^{1/2}g(X), \tag{12a}$$
or
$$r = 1 + \epsilon g(X), \tag{12b}$$
according to whether the obstacle is on the tube axis or there is a local undulation of the tube wall.

If the flow is near resonance, i.e. $C_n = 1 - \epsilon\Delta$, the GY equation for $A \equiv A_n(X, T)$ is
$$-\frac{2I_n j_n^3}{|2\Omega|}\left\{\int_{-\infty}^{X} K(A, A')\frac{\partial A'}{\partial T}\,\mathrm{d}X' + \Delta A\right\} + I_n A_{XX} - \tfrac{1}{2}j_n g^2\left(1 + \frac{j_n^2 A}{|2\Omega|}\right) = 0, \tag{13a}$$
when there is an obstacle on the tube axis or
$$-\frac{2I_n j_n^3}{|2\Omega|}\left\{\int_{-\infty}^{X} K(A, A')\frac{\partial A'}{\partial T}\,\mathrm{d}X' + \Delta A\right\} + I_n A_{XX} + |2\Omega| J_0(j_n) g\left(1 + \frac{j_n^2 J_0(j_n) A}{|2\Omega|}\right) = 0, \tag{13b}$$
when there is an undulation of the tube wall.

Here, Ω is given by (6) ($\Omega = \frac{1}{2}j_n$ and I_n, A' and $K(A, A')$ are defined by
$$I_n = \tfrac{1}{2}J_0^2(j_n), \quad A' = A'(X', T), \tag{14a, b}$$
and
$$K(A, A') = \frac{|2\Omega|}{2I_n j_n}\left\{\int_0^{C_n/2}\left(\frac{r}{r'} + \frac{r'}{r}\right)\frac{\partial r}{\partial A}\frac{\partial r'}{\partial A'}\,\mathrm{d}\phi + \int_0^{C_n/2}\left[\frac{1}{r'}\frac{\partial r'}{\partial A'}\frac{\partial}{\partial \phi}\left(r\frac{\partial r}{\partial A}\right) + \frac{1}{r}\frac{\partial r}{\partial A}\frac{\partial}{\partial \phi}\left(r'\frac{\partial r'}{\partial A'}\right)\right]\phi\,\mathrm{d}\phi\right\}. \tag{14c}$$
Note that a new variable $\phi = \phi(r, A)$ is introduced, which is defined by
$$\phi = \tfrac{1}{2}C_n r^2 + A(X, T) f_n(r), \tag{15}$$
and is used as an independent variable instead of r. For the existence of the inverse $r = r(\phi, A)$, the condition
$$\frac{\phi_r}{r} = C_n + \frac{A}{r}\frac{\mathrm{d}f_n}{\mathrm{d}r} \neq 0, \tag{16a}$$
must be satisfied for all $r(0 \leqslant r \leqslant 1)$ by virtue of the implicit function theorem. Using (10*b*), this is equivalent to
$$A \neq -\frac{C_n}{j_n J_0(j_n r)} \quad \text{for all} \quad r(0 \leqslant r \leqslant 1), \tag{16b}$$

or
$$-\frac{C_n}{j_n} < A < \frac{C_n}{j_n |J_0(j_1)|}, \tag{16c}$$

where $J_0(j_1) = -0.40276$. (The upper bound of A given by Grimshaw & Yi (1993) (see their (3.25)) is C_n/j_n, or, more precisely, they used $C_1/(j_1|J_0(j_1)|)$ for the first ($n = 1$) mode. For the general nth mode, it is replaced by $C_n/(j_n|J_0(j_1)|)$ and becomes about 2.5 times larger compared to C_n/j_n.) By comparison of (15) with (10a), we see that ϕ given by (15) is equal to the total stream function with an error of $O(\epsilon)$. Then, (16a, b) or (16c) is approximately identical to the condition for the absence of the axial flow reversal. We should note that, in (16c), the violation of the lower limit of A leads to the axial flow reversal on the tube axis ($r = 0$), while the violation of the upper limit of A leads to the axial flow reversal at $r = j_1/j_n$, which corresponds to the tube wall ($r = 1$) for the first radial mode ($n = 1$). Since the modulus of $C_n/(j_n|J_0(j_1)|)$ is about 2.5 times larger than that of $-C_n/j_n$, we can expect that the axial flow reversal is most likely to occur at the tube axis when the A becomes smaller than $-C_n/j_n$. Finally, it is of interest to note that the forcing term in (13a) vanishes when A reaches the lower limit of (16c). Even if A does not reach the lower limit, the forcing term becomes smaller with the reduction of $A(<0)$. Similarly, the forcing term in (13b) vanishes for mode $n = 1$ when A reaches the upper limit of (16c). Even A does not reach the upper bound, the forcing term becomes smaller with the growth of $A(>0)$. These show that the time development of the wave becomes much slower as the amplitude reaches the breaking point, i.e. as the flow reversal is approached. This also suggests that after the flow reversal occurs, the wave amplitude does not change significantly in the region where the flow reversal has occurred.

3. Numerical method

We calculate the flow in the region of $-40 \leqslant x \leqslant 60$ and $0 \leqslant r \leqslant 1$, with the deformation of the boundary localized near $x = 0$. The numerical method is the same as in the previous papers (Hanazaki 1991, 1993a) and is summarized in the Appendix. However, some discussions about the boundary conditions are appropriate here. In this study, free-slip condition is generally used on both the obstacle surface and the tube wall to exclude the effect of the boundary layer. An exception is the boundary condition for the azimuthal velocity w on the tube wall, where the condition of a 'rotating tube': $w = r\Omega$, with r the radius of the tube taken account of the deformation of the tube wall, was used.

In the previous numerical studies for the vortex breakdown, free-slip boundary conditions were often used for the axial velocity u. The constant azimuthal velocity w based on the conservation of circulation $\Gamma(= rw = \Omega)$ along the straight tube wall was also often used (e.g. Kopecky & Torrance 1973) on the assumption that the decrease of circulation along the tube wall owing to viscosity is negligible. Those simulations were done for the Burgers-vortex type rotation and the azimuthal velocity w on the tube wall was in general not large, because in that case the azimuthal velocity decreases proportional to r^{-1}, where r is large. Then the differences from the laboratory experiments which exclusively used the non-rotating tube (no-slip conditions) were thought to be small. The differences which come from the free-slip conditions for u (and v) would be also small as tested by Kopecky & Torrance (1973).

In the case of the uniform (solid-body) rotation the azimuthal velocity increases in proportion to r, i.e. the distance from the tube axis. However, in the previous experiments for the uniform (solid-body) rotation, the tube wall has been always

'rotated' with the angular velocity Ω because the rotation is necessary for the generation of the 'uniformly' rotating fluid (Long 1953; Pritchard 1968, 1969). Therefore, the boundary condition for the azimuthal velocity in the experiments is $w = r\Omega$, exactly the one used in this numerical study. We note here that, although we did not use the free-slip conditions, our tests showed that the free-slip condition for the azimuthal velocity on the tube wall makes only negligible differences to the solution. The circulation on the tube wall ($\Gamma = rw = \Omega$) is conserved if the viscosity effect is negligible or if the rotation is uniform (see equation (2*a*)), then the value of w at the upstream end of the tube wall $w = 1 \times \Omega$ is only slightly changed along the tube wall as far as the deformation of the tube wall is small.

The experiments for the uniform rotation have been carried out by moving the obstacle along the tube axis, which means that the boundary condition on the tube wall is $(u, v) = (U, 0)$ if we look at the velocities from the moving (obstacle) frame. This condition is more similar to the free-slip condition than the no-slip condition except when the wave amplitude is extremely large and the flow reversal occurs on the tube wall. But this would rarely occur. Then the use of the free-slip conditions for u and v is reasonable also from this point of view.

Note also that there is an inconsistency in the boundary condition at the upstream end of the tube wall if we use the no-slip condition, since the boundary condition at the inflow gives $u = U$, $w = b\Omega$, while the no-slip condition on the tube wall gives $u = w = 0$. This is one of the reasons why in the previous numerical studies, free-slip boundary conditions have been used (Kopecky & Torrance, 1973).

When there is an obstacle on the tube axis, the boundary conditions on the obstacle also become problematic. We have used in this study the free-slip conditions. This would cause some quantitative differences from the laboratory experiments which used a non-rotating obstacle. However, in the experiments of Pritchard (1968, 1969) the sphere on the tube axis was also rotated with the angular velocity Ω, the same angular velocity as the tube wall. This was done to suppress the development of the Ekman boundary layer on the sphere surface. The purpose of the previous experiments and this study is 'not' in the study of the boundary-layer development which would obscure the essential mechanisms of the inertial waves. So we have used the free-slip boundary condition on the obstacle surface. Indeed, the use of the free-slip conditions in this study has given the distributions of azimuthal velocity on the obstacle surface much more similar to the rotating obstacle than the non-rotating obstacle. This is the reason why Pritchard (1968, 1969) could avoid the development of the boundary layer in his experiments by rotating the sphere. We should also note that, if the circulation $\Gamma = rw$ is approximately conserved because the Reynolds number is large and the flow has relatively uniform rotation, $\Gamma = 0$ on the obstacle surface. This is because the contour of Γ on the obstacle surface originates from the tube axis ($r = 0$) in the more upstream region. In the experiments of Taylor (1922), the rotation of a light sphere, which was allowed to rotate freely, was negligible except when the Taylor column exists. If there is a Taylor column, it forms a closed streamline and a flow separation occurs on the obstacle surface, allowing that the contour of Γ does not necessarily originate from the tube axis. Then the rotation of the sphere becomes much faster (see Batchelor 1967, p. 565) if the Taylor column exists. The azimuthal velocity on the obstacle surface is originally small if the fluid rotation is not fast and the Taylor column does not exists. We can also consider the free-slip condition for the azimuthal velocity as identical to the condition that the light obstacle is allowed to rotate freely.

We still have to admit that the use of the free-slip condition for u and v on the obstacle surface gives quantitative differences in the solution from the experiments

where the no-slip conditions are applied. However, Pritchard reports that the boundary-layer development was sufficiently suppressed only by rotating the sphere, showing that the effect of the boundary layer generated by the no-slip conditions for u and v was small.

We have used in this study either the obstacle located on the tube axis whose shape is given by

$$r_{in} = 0.05\ \mathrm{sech}^2(0.4x), \tag{17a}$$

or the deformation of the tube wall given by

$$r_{out} = 1 + h\,\mathrm{sech}^2(0.4x), \tag{17b}$$

with h being the maximum radial amplitude of the tube wall deformation whose sign denotes the expansion or the contraction. Specifically h was $+0.005$, -0.005 or -0.015. An exception is the use of the short obstacle on the tube axis whose shape is given by

$$r_{in} = 0.05\ \mathrm{sech}^2(4x). \tag{17c}$$

This short obstacle was used for the calculations of the subcritical flows, since the long obstacle did not excite lee waves of short wavelength and became inconvenient to identify the lee wavelength for comparison with the previous laboratory experiments.

The Reynolds number is $Re = 10^4$ unless otherwise stated. This value is used to avoid the strong viscous damping of the inertial waves. As has been discussed in the previous paper (Hanazaki 1993*a*), we have tested the cases of various Reynolds numbers and found that, above $Re = 5000$, the generation period of the upstream-advancing waves in the critical and subcritical flows in non-uniformly rotating (Burgers-type vortex) flows are almost independent of the Reynolds number.

The Froude number F is below $F = 1.05$, so that the flow is near resonance or subcritical to the fastest (lowest) mode ($n = 1$). We investigate mainly the flow near $F = 1$, for which the wave of mode $n = 1$ is near resonance. For comparison with the linear theories and the previous experiments for the inertial waves, the upstream wave propagation speed and the lee wavelength in the subcritical flow ($0.5 \leqslant F \leqslant 0.9$) were also investigated.

The boundary conditions at the upstream boundary are

$$u = 1, \quad v = 0, \quad w = r\Omega, \tag{18a}$$

and the boundary conditions on the downstream boundary are

$$\frac{\partial \boldsymbol{v}}{\partial t} + u\frac{\partial \boldsymbol{v}}{\partial x} = 0. \tag{18b}$$

Since the upstream boundary conditions are fixed, the computation can be done only until the upstream-advancing waves reach the upstream boundary. This limitation can be predicted by linear theory, i.e. using the upstream propagation speed of the fastest ($n = 1$) mode in its long-wave limit ($k = 0$):

$$C_1 - 1 = \frac{1}{F} - 1. \tag{19}$$

However, we should note that the tube length ($= 100$) in this study is much longer compared to the previous numerical studies for the vortex breakdown where it was usually about 3–10. Therefore, the effect of the upstream influence is completely

avoided near the upstream boundary as far as the waves do not reach the upstream boundary. Then the setting of the fixed boundary conditions does not make any difference to the solution obtained by other boundary conditions, e.g. the ones which set the axial derivatives to be zero ($\partial v/\partial x = 0$) at the upstream boundary.

To compare the solutions of the Navier–Stokes equations with the theory, the GY equation was solved by the same method as used in Hanazaki (1992, 1993*b*), which is the finite-difference analogue of the spectral method used by Yi & Warn (1987).

4. Results

We first show the solutions of the Navier–Stokes equations for the flow past an obstacle on the tube axis. The obstacle shape is given by equation (17*a*). In figure 3, we show the Stokes streamlines in the whole computed region at the last stage ($t = 200$) of the time development. Note that the axial length is 1/100 of the radial length. When $F = 0.9$ ($F < 1$, i.e. $C_1 > 1$) (figure 3*a*), the phase and the group velocity of the mode $n = 1$ wave in their long-wave limit is larger than the axial flow velocity. Then the upstream-advancing long waves appear and their propagation speed is given by (19) as 0.111. When $t = 200$ this gives the foremost position of the upstream wave as 22.2, in agreement with figure 3(*a*) (cf. figures 4*a* and 5*a*). At this Froude number the flow is slightly subcritical and the amplitudes of the upstream and the downstream waves are not very large. When $F = 0.95$ (figure 3*b*), the flow is still slightly subcritical but becomes nearly resonant. Then the wave amplitude becomes largest among all the Froude numbers used in this study. The advancing speed of the upstream waves becomes slower owing to the reduction in the linear long-wave speed. When $t = 200$, equation (19) predicts the position of the foremost wave as $0.0526 \times 200 = 10.526$, which is in agreement with figure 3(*b*) (cf. figures 4*b* and 5*b*). In the case of $F = 1.0$ (figure 3*c*), the upstream flow is exactly resonant to the first inertial-wave mode ($n = 1$) and the solutions of the linearized equation diverge. In this case there is no upstream propagation of the inertial waves. This confirms that the nonlinear correction of the wave speed in the uniformly rotating fluid is very small as has been shown in Hanazaki (1991). It will take an indefinitely long time even if we could identify some upstream influence of the obstacle. When $F = 1.05$ ($F > 1$, i.e. $C_1 < 1$) (figure 3*d*), the flow becomes supercritical to all the modes with no upstream waves and only weak downstream waves.

To see the time development of the inertial waves clearly, it is appropriate to calculate the amplitude of the mode $n = 1$ component of the wave which corresponds to the solution of the GY equation. We have computed the amplitude of the nth mode $A_n(x, t)$ by the following method. We first assume that the total stream function can be written as (10*a*). Then using the orthogonality condition for the Bessel function of the first kind of order one:

$$\int_0^1 \mathrm{d}r\, r J_1(j_m r) J_1(j_n r) = \delta_{mn} \tfrac{1}{2} J_2(j_m)^2, \tag{20a}$$

$A_n(x, t)$ is calculated approximately as

$$A_n(x, t) = \frac{2 \int_0^1 \mathrm{d}r (\psi - \Psi(r)) J_1(j_n r)}{J_2(j_n)^2}, \tag{20b}$$

with an error of $O(\epsilon)$. By substituting $n = 1$ into (20*b*), the first mode component

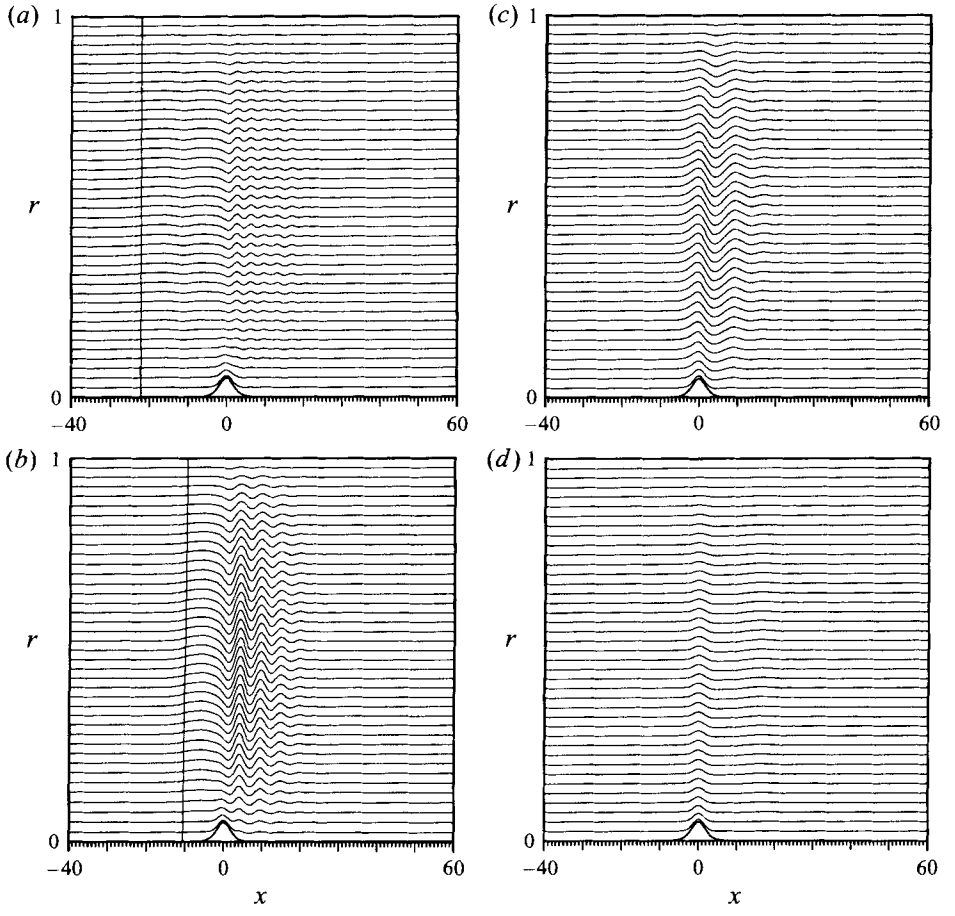

FIGURE 3. Stokes streamlines at time $t = 200$ obtained by the solution of the Navier–Stokes equations ($Re = 10^4$). The waves are excited by an obstacle on the tube axis whose shape is given by (17a). The streamlines are drawn for $\psi = 3.125 \times 10^{-4} \times n^2$ ($0 \leqslant n \leqslant 40$): ($a$) $F = 0.9$; (b) $F = 0.95$; (c) $F = 1.0$; (d) $F = 1.05$. The vertical lines in (a) and (b) show the position of the foremost wave predicted by the linear theory (19).

$A_1(x, t)$ is obtained. The result is shown in figure 4, where the sign of the amplitude $A(x, t) = A_1(x, t)$ is reversed.

We see in figure 4 that upstream advancing waves appear only when $F < 1$ ($C_1 > 1$), although there is a growing wave near the obstacle ($x \approx 0$) when $F = 0.95$ and $F = 1.0$. When $F = 1.05$, the wave near the obstacle becomes steady and the wave amplitude does not grow after the amplitude has reached a constant value. In this case there is a depression just downstream of the obstacle which becomes longer with time. We see in figures 4(a) and 4(b) that the foremost end of the upstream wave, which has the long wavelength ($k = 0$), propagates almost at a constant speed from $x = 0$ as predicted by the linear theory (19).

The results described above show that the nonlinear correction of the linear wave speed is very small if the flow has a uniform rotation. This is very different from the resonant solutions for non-uniform (Burgers-vortex type) rotation (Hanazaki 1991, 1993a), where definite increase of the propagation speed of the upstream waves owing to the nonlinearity was found. In that case there is an additional speed

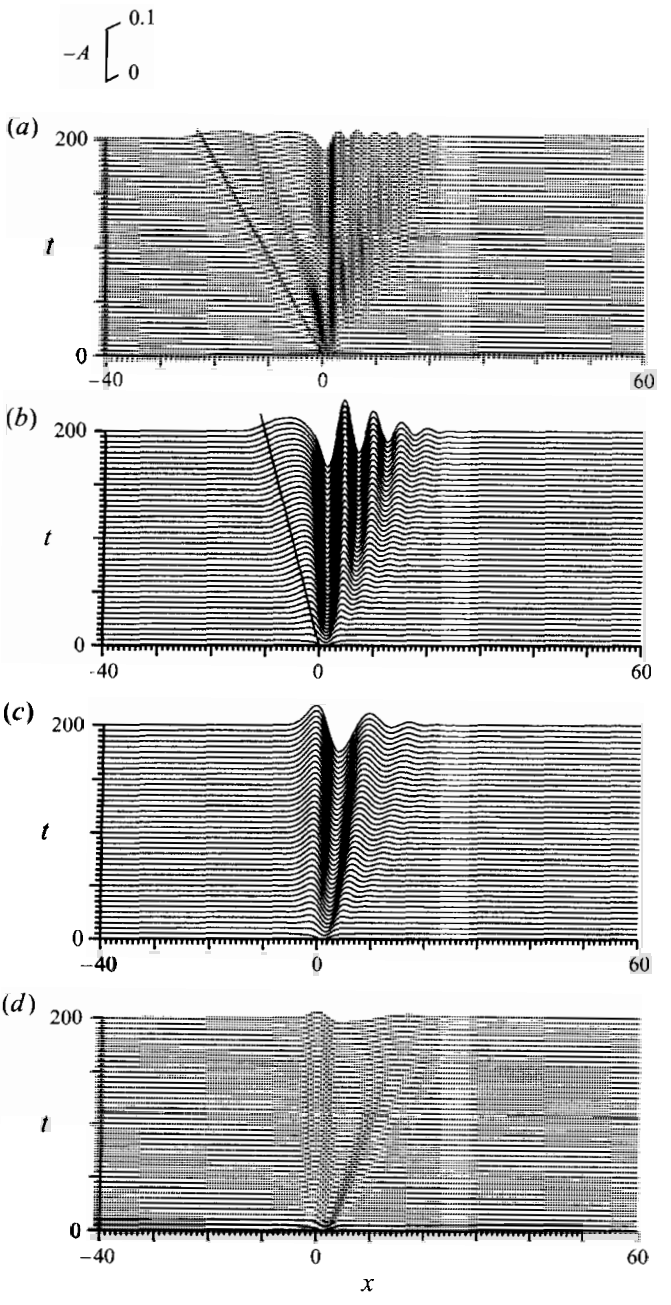

FIGURE 4. Time development of $A = A_1(x, t)$ obtained from the solution of the Navier–Stokes equations ($Re = 10^4$). The waves are excited by an obstacle on the tube axis (17*a*): (*a*) $F = 0.9$; (*b*) $F = 0.95$; (*c*) $F = 1.0$; (*d*) $F = 1.05$. Note that the sign of A is reversed in this figure. The straight lines in (*a*) and (*b*) show the position of the foremost wave predicted by the linear theory (19).

proportional to the amplitude of the upstream solitary wave and the upstream influence was found even when the Froude number is $F = 1.1$ (> 1).

The wavelength λ_s of the standing lee waves downstream of the obstacle can also be predicted by the linear theory (8). For the first mode ($n = 1$, $C_1/U = 1/F, j_1 = 3.83171$) this gives $\lambda_s = 3.39$ when $F = 0.9$, and $\lambda_s = 4.98$ when $F = 0.95$. These values agree

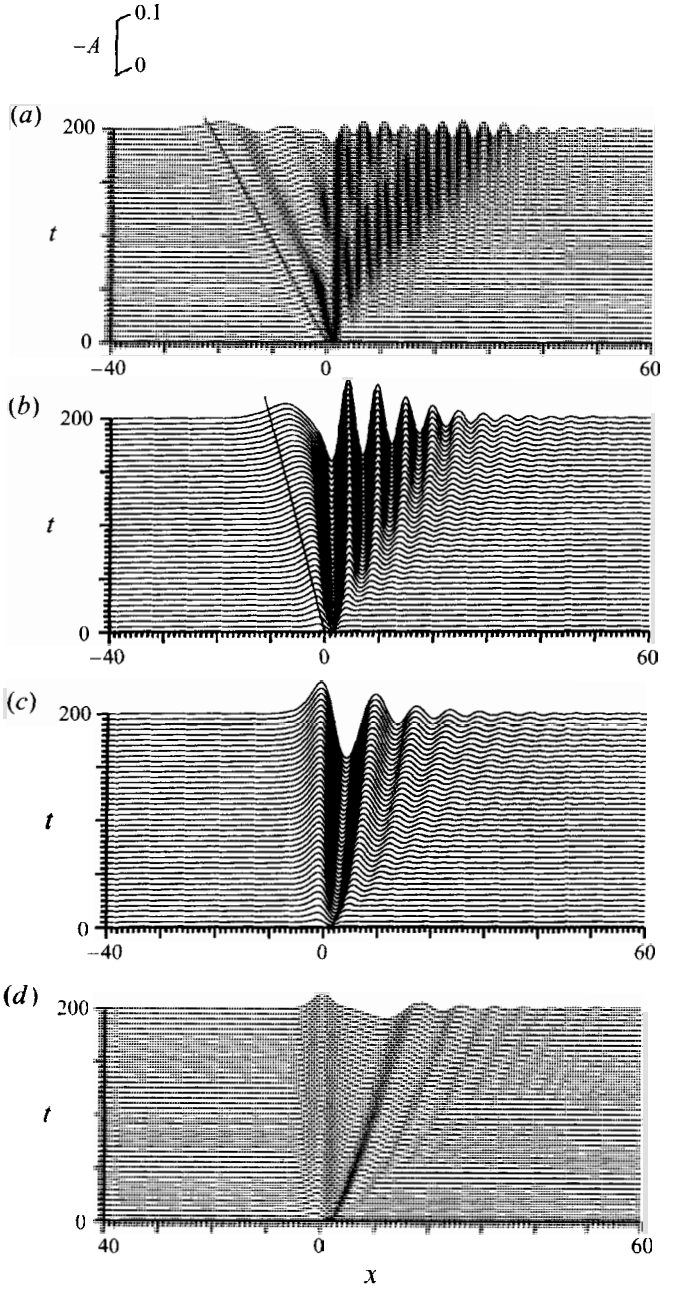

FIGURE 5. Time development of $A(x, t)$ obtained from the solution of the GY equation. The waves are excited by an obstacle on the tube axis (17*a*): (*a*) $F = 0.9$; (*b*) $F = 0.95$; (*c*) $F = 1.0$; (*d*) $F = 1.05$. The straight lines in (*a*) and (*b*) show the position of the foremost wave predicted by the linear theory (19).

with figures 3(*a*, *b*) and 4(*a*, *b*). It is of interest that the linear theory can predict the wave speed and the wavelength without large errors even when the Froude number is close to one, although the solution of the linearized equation diverges and we cannot obtain the non-divergent solution when $F = 1.0$.

In figure 5 we show the solutions of the Grimshaw–Yi equation which correspond

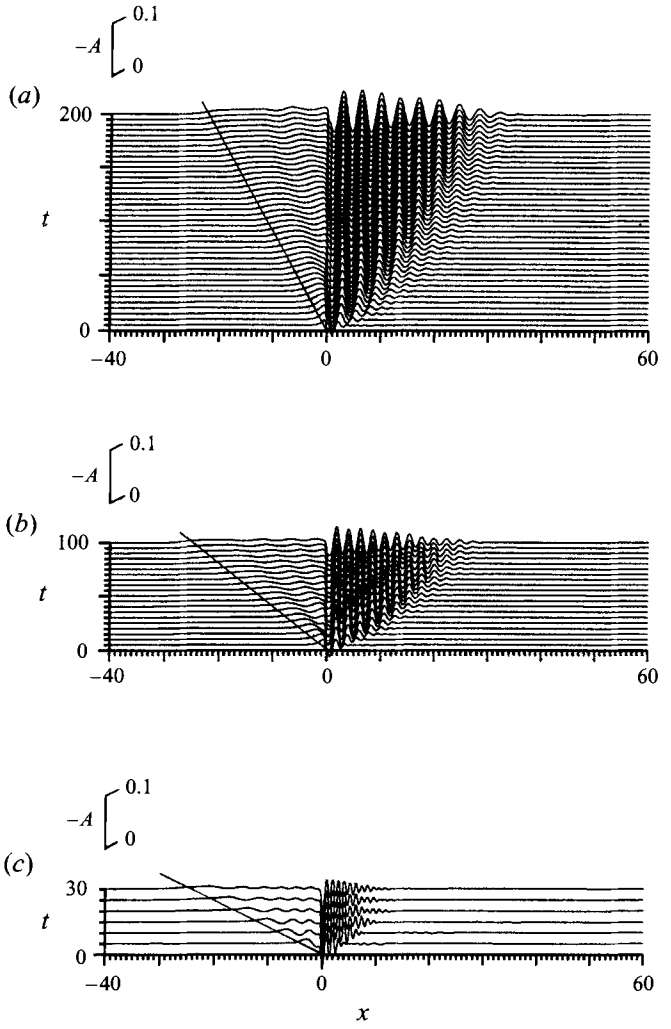

FIGURE 6. Time development of the first mode $A = A_1(x, t)$ obtained from the solution of the Navier–Stokes equations for subcritical ($F < 1$) flows ($Re = 10^4$). The waves are excited by a 'short' obstacle on the tube axis (17*c*): (*a*) $F = 0.9$; (*b*) $F = 0.8$; (*c*) $F = 0.546\,17$. The straight lines show the position of the foremost wave predicted by the linear theory (19).

to figure 4. In this study, the value of ϵ is set to be $\epsilon = 0.01$ in all the solutions of the Grimshaw–Yi equation. The qualitative agreement in the dependence on the Froude number is very good. The agreement is good even quantitatively, except that in the solutions of the Navier–Stokes equations (figure 4), the amplitude of the far downstream waves ($x \geqslant 20$) are smaller owing to the viscosity of the fluid, and the amplitude near the obstacle is also smaller. A typical feature of the subcritical flow is the initial upstream-propagation of the standing downstream waves, which was first observed in the flow of a linearly stratified Boussinesq fluid (Grimshaw & Yi 1991; Hanazaki 1993*b*). This is observed when $F = 0.9$ (figure 5*a*), where we see the initial ($0 < t < 100$) slight upstream movement of the downstream waves ($0 < x < 10$). This can be also identified in the corresponding solution of the Navier–Stokes equations (figure 4*a*).

To clarify the applicability of the linear theory to the subcritical flows, the

Navier–Stokes equations for lower Froude numbers were solved. In figure 6, the time developments of the amplitude of mode $n = 1$ are presented for $F = 0.9$, 0.8 and 0.546 17. In the case of $F = 0.546\,17$, the second mode $n = 2$ is at resonance. A short obstacle given by (17*c*) is used here instead of (17*a*). The axial length of the obstacle is then one tenth of (17*a*). If the long obstacle (17*a*) is used, the wave components of short wavelength are very weakly excited because only the wavenumber components which exist in the Fourier transformed spectrum of the obstacle shape can be excited, at least under the assumption of the linearity of the wave (McIntyre 1972). Indeed, if the Froude number becomes small ($F \approx 0.6$) and the lee wavelength becomes short, it becomes difficult to identify the lee wavelength for comparison with the linear theory if we use (17*a*) as the obstacle. Even in the case of $F = 0.9$, where the Froude number is still near one and the lee wavelength is not very short ($\lambda_s = 3.39$), the lee wave amplitude in figure 4(*a*), which used a long obstacle (17*a*), is much smaller than that in figure 6(*a*), where a short obstacle (17*c*) is used. The same is true of the difference in the wavenumber components of the upstream wave. The amplitude of the upstream wave is similar in figures 4(*a*) and 6(*a*) ($F = 0.9$) because the upstream waves generated early have long wavelengths. However, as the Froude number decreases and the shorter waves begin to propagate upstream earlier as shown in figure 6(*c*) ($F = 0.546\,17$), differences in the upstream wave also become much larger because the long obstacle (17*a*) cannot excite 'short' upstream waves and the generation of the upstream waves almost ceases much earlier compared to figure 6(*c*). Therefore, we have used here a short obstacle given by (17*c*) to clarify the effect of the short waves.

The upstream-advancing speeds of the foremost long ($k = 0$) wave of mode $n = 1$ agree with the linear theory (19). The predicted speed is 0.111 when $F = 0.9$, 0.25 when $F = 0.8$ and 0.831 when $F = 0.546\,17$. These are shown in figure 6 as straight lines.

If is of interest to note that the 'shortest' wavelength in the upstream wave λ_0 ($= 2\pi/k_0$) (see figure 2*a*) can also be predicted by the linear theory. It is determined by the condition that the axial group velocity is equal to the axial flow velocity:

$$C_g(k_0) = \frac{2b\Omega j_1^2}{(j_1^2 + b^2 k_0^2)^{3/2}} = U. \tag{21a}$$

Rewriting (21*a*) using the Froude number F defined by (6) and (7), the limit wavelength λ_0 is obtained as

$$\lambda_0 = \frac{2\pi}{j_1\left(\dfrac{1}{F^{2/3}} - 1\right)^{1/2}}. \tag{21b}$$

This gives $\lambda_0 = 6.08$ when $F = 0.9$, $\lambda_0 = 4.09$ when $F = 0.8$ and $\lambda_0 = 2.33$ when $F = 0.546\,17$. The wavelengths of the shortest upstream waves indeed approach these limit values in figure 6.

Note that the amplitude of the upstream wave is generally small in figure 6 compared to the lee wave since the short obstacle excites mainly the waves of short wavelength, which can appear as the large-amplitude lee waves but cannot appear initially in the upstream waves. This is one of the reasons why in the laboratory experiments by Long (1953) upstream waves were not observed. In his experiments the obstacle length is comparable to the tube radius. In that case, long wavelength components, which should appear earlier in the upstream region, become small. To identify the small-amplitude waves, other experimental methods have to be used as was done in a similar dynamical system of stratified flows. In stratified flows, the visualization of the 'disturbance streamlines' of the whole field, which was originally quiescent, was

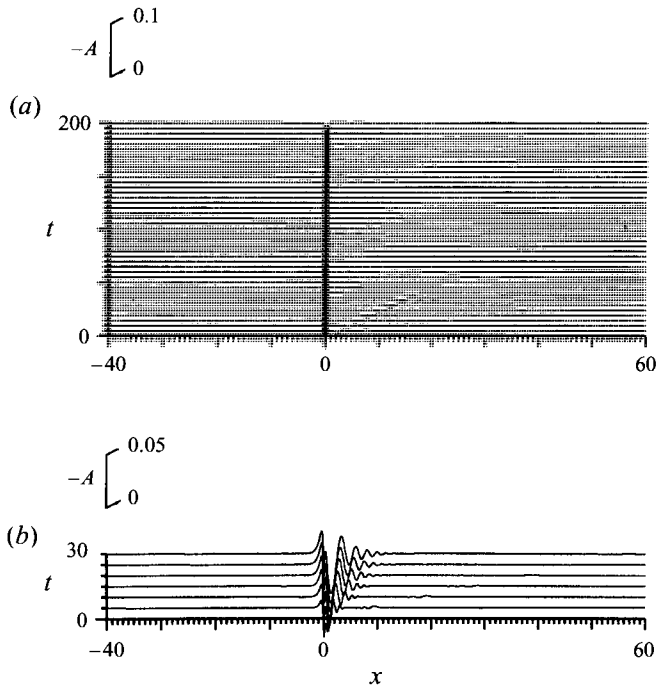

FIGURE 7. Time development of the second mode $A = A_2(x, t)$ obtained from the solution of the Navier–Stokes equations for subcritical ($F < 1$) flows ($Re = 10^4$). The waves are excited by a 'short' obstacle on the tube axis (17*c*): (*a*) $F = 0.9$; (*b*) $F = 0.54617$.

carried out by Baines (1979) and the measurement of the upstream disturbance velocity was made by Castro & Snyder (1988).

We next show the effect of the second ($n = 2$) mode when $F \leqslant 1$. The amplitude of the second mode $A = A_2(x, t)$ was calculated using (20*b*) with $n = 2$. The results are shown for $F = 0.9$ and $F = 0.54617$ in figure 7. Note that the condition $F = U/C_1 = Uj_1/2b\Omega = 0.54617$ is identical to $C_2 = 2b\Omega/j_2 = U$ ($j_2 = 7.01559$), i.e. the resonant condition of the second mode. Then, if the Froude number is $F = 0.9$, the flow is supercritical to the second mode and thus A_2 is not excited at all in figure 7(*a*) except that the components of the 'obstacle shape' appear very near the obstacle ($x \approx 0$). On the other hand, if $F = 0.54617$, the flow is critical (resonant) to the second mode and a large A_2 is excited near the obstacle (figure 7*b*). The resonant wave patterns of mode $n = 2$ shown in figure 7(*b*) are similar to the resonant profiles of mode $n = 1$ shown in figure 4(*c*), although the wavelength is shorter in figure 7(*b*).

To summarize the dependence of the lee wavelength of mode $n = 1$ components on $U/\Omega b$ ($= 2F/j_1 = 0.522F$), the wavelengths obtained from the solution of the Navier–Stokes equations are shown in figure 8. The computational results for $F = 0.7$, 0.6 and 0.5 are also included here and the comparisons are made with the experiments by Long (1953) and Pritchard (1968, 1969) and also with the linear theory (8). The agreement is generally good except that the numerical results give slightly longer wavelengths compared to the linear theory.

We next consider the waves excited by a local contraction of the tube wall. Here, we have used the contraction shape given by (17*b*) with $h_1 = -0.005$. In figure 9, we show the overall streamlines when $F = 0.95$ ($t = 200$). Note here that even a very small undulation of the wall (in this case, only 0.5% of the tube radius) causes a wave of very

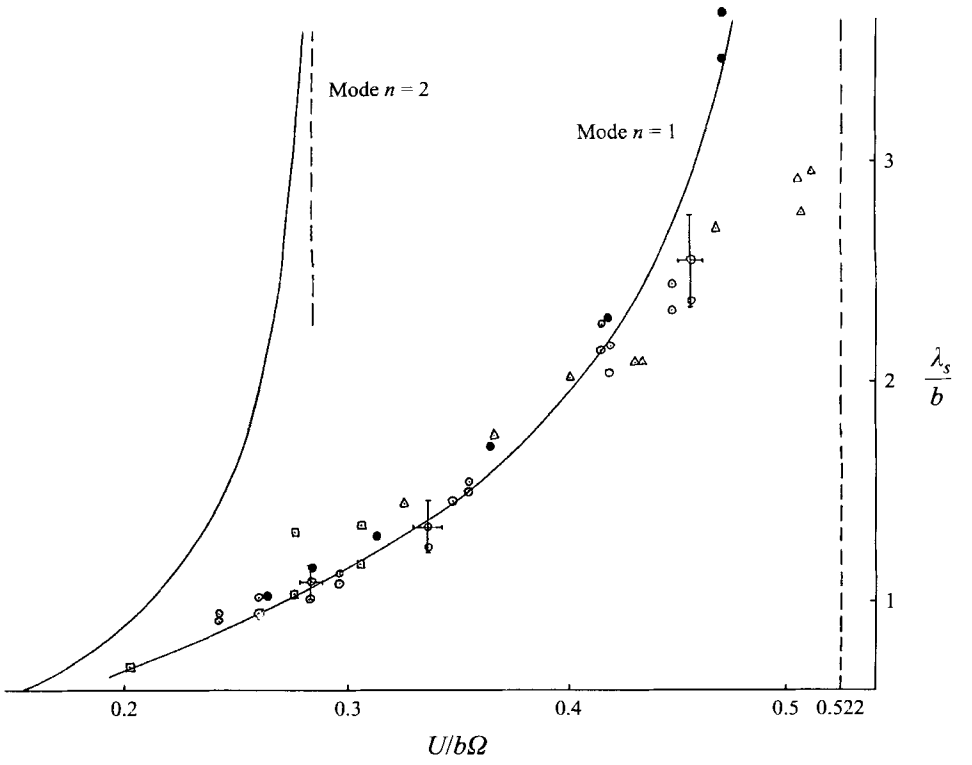

FIGURE 8. Comparison of the lee wavelength. The solutions of the Navier–Stokes equations: ●, the experiments by Long (1953): □, the experiments by Pritchard (1968); △, (sphere radius/tube radius = 0.275); ○, (sphere radius/tube radius = 0.226).

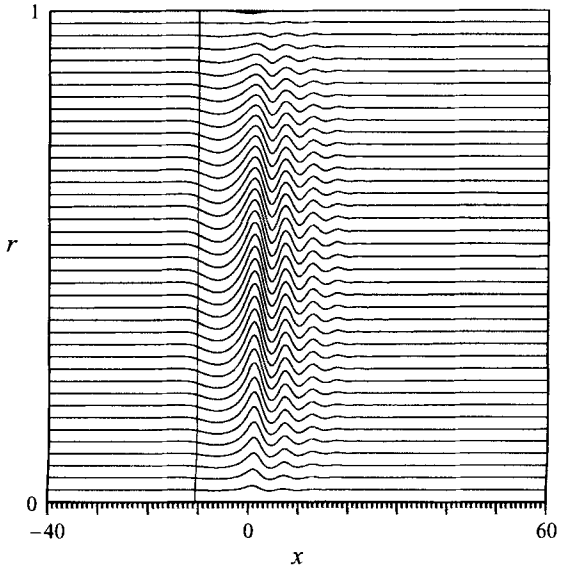

FIGURE 9. Stokes streamlines at the time of $t = 200$ ($F = 0.95$) obtained by the solution of the Navier–Stokes equations ($Re = 10^4$). The waves are excited by a local contraction of the tube wall given by (17b) with $h = -0.005$. Streamlines are drawn for $\psi = 3.125 \times 10^{-4} \times n^2$ ($0 \leqslant n \leqslant 40$).

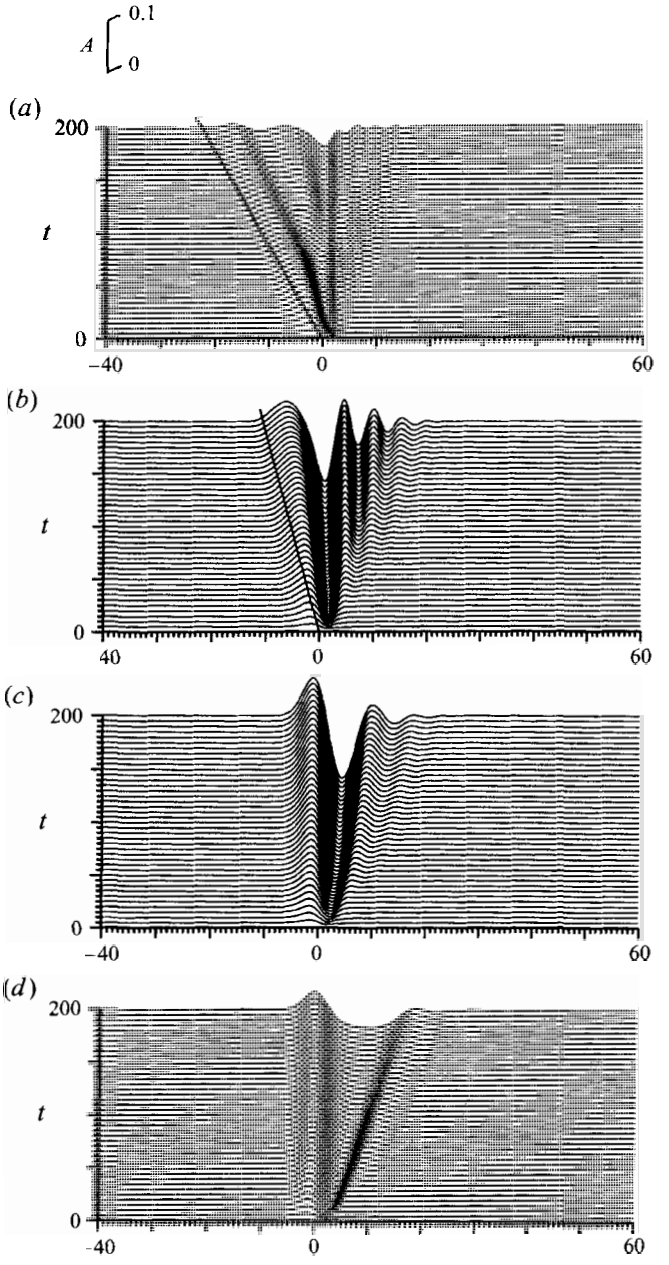

FIGURE 10. Time development of $A = A_1(x, t)$ obtained from the solution of the Navier–Stokes equations ($Re = 10^4$). The waves are excited by a local contraction of the tube wall given by (17*b*) with $h = -0.005$. (*a*) $F = 0.9$; (*b*) $F = 0.95$; (*c*) $F = 1.0$; (*d*) $F = 1.05$. The straight lines in (*a*) and (*b*) show the position of the foremost wave predicted by the linear theory (19).

large amplitude in a long time if the flow is near resonance. This is because, in the case of the tube wall deformation, the radial undulation is scaled by ϵ instead of $\epsilon^{1/2}$, as shown in (12*b*). This level of undulation of the tube wall, which corresponds to the undulation of 0.25 mm for a tube with a radius of 5 cm, may occur in usual laboratory experiments for swirling flows and this suggests the possibility that some results of the

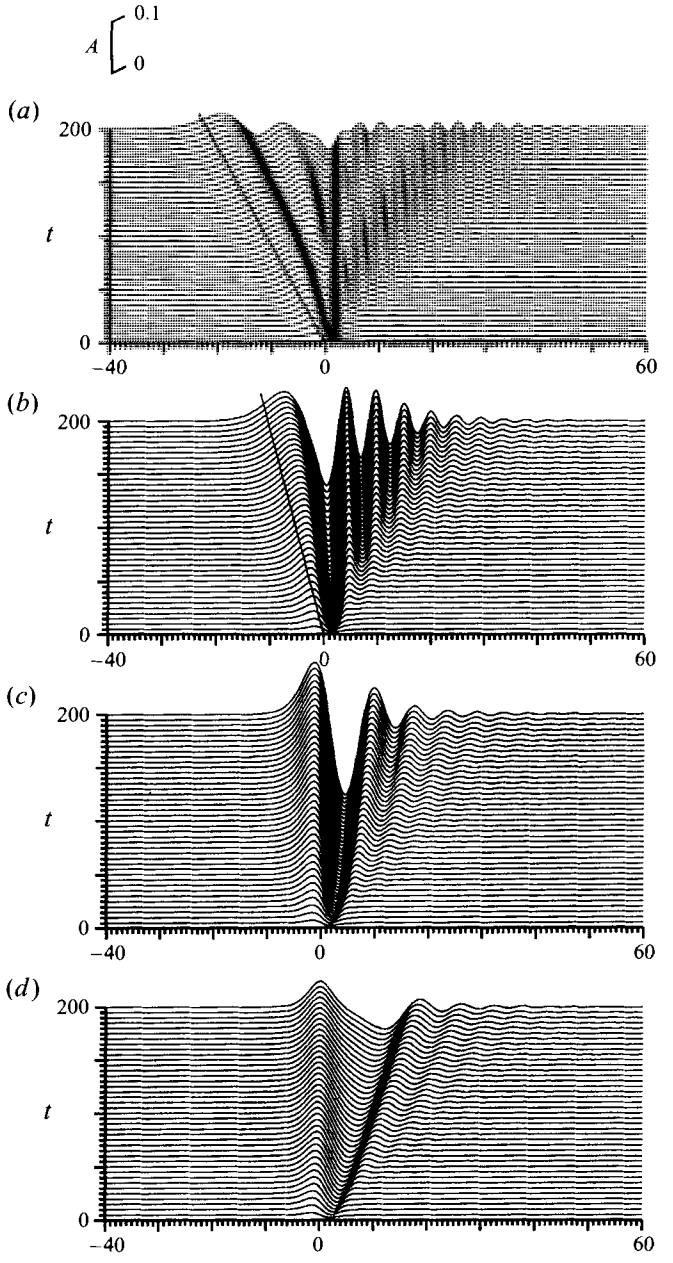

FIGURE 11. Time development of $A = A_1(x, t)$ obtained from the solution of the GY equation. The waves are excited by a local contraction of the tube wall given by (17*b*) with $h = -0.005$. (*a*) $F = 0.9$; (*b*) $F = 0.95$; (*c*) $F = 1.0$; (*d*) $F = 1.05$. The straight lines in (*a*) and (*b*) show the position of the foremost wave predicted by the linear theory (19).

previous experiments could be affected by an unexpected and undesirable very small undulation of the tube wall.

In figures 10 and 11, we show the time developments of $A = A_1(x, t)$ obtained from the solution of the Navier–Stokes equations and the solution of the GY equation. As in the case of the waves excited by an obstacle located on the tube axis (figures 4 and 5), the qualitative agreement is very good, although some quantitative differences are

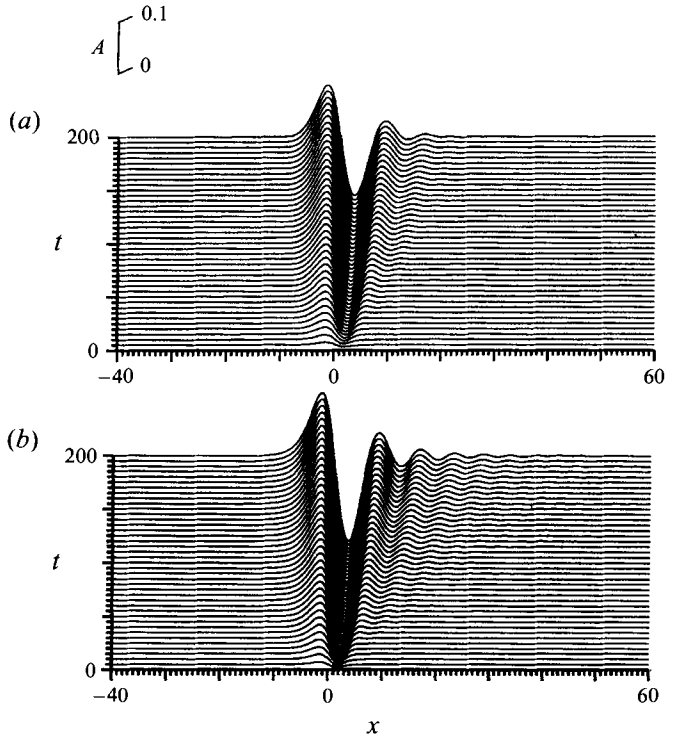

FIGURE 12. Time development of $A = A_1(x, t)$ when the waves are excited by a local expansion of the tube wall given by (17*b*) with $h = 0.005$ ($Re = 10^4$, $F = 1.0$). (*a*) Navier–Stokes equations; (*b*) GY equation ($\epsilon = 0.01$).

observed. The qualitative dependence of the wave patterns on the Froude number is the same as in figures 4 and 5, the only major difference being the sign of A. In the forcing terms of the GY equation (13*a*) and (13*b*), i.e. $-j_n g^2(1+j_n^2 A/|2\Omega|)/2$ and $|2\Omega|J_0(j_n)g(1+j_n^2 J_0(j_n)A/|2\Omega|)$, the terms in parentheses must be always positive because of the constraint of (16*c*). Therefore, the sign of the forcing term is always negative in (13*a*), while it is determined by the sign of $J_0(j_n)g$ in (13*b*). The function $g(X)$ is negative for the contraction of the tube wall, while it is positive for the expansion of the tube wall. The value of $J_0(j_n)$ is negative when n is an odd number and positive when n is an even number. Then $J_0(j_1)g$ is positive for the contraction ($g < 0$) of the tube wall. After all, the sign of the forcing term is always negative for the obstacle on the tube axis (figures 3, 4 and 5), while it is positive for a contraction of the tube wall (figures 9, 10 and 11). In addition, in the weakly nonlinear limit $|A| \to 0$, the kernel $K(A, A')$ asymptotes to one ($K(A, A') \to 1$) and the GY equation becomes the fKdV equation as noted by Grimshaw & Yi (1993). Therefore, in the weakly nonlinear limit, GY equations (13*a*) and (13*b*), respectively, reduce to the fKdV equations with a negative and a positive forcing, so that the resultant $A(x, t)$ takes the opposite sign, at least for the initial time development.

In figure 12, the time development of $A = A_1(x, t)$ obtained from the Navier–Stokes equations and the GY equation are given for the wave excited by a local expansion of the tube wall. Here, the value of $J_0(j_1)g(X)$ is negative so that the sign of $A(x, t)$ is the same as the waves excited by an obstacle on the tube axis. We see again the agreement including the wavelength, although the amplitude is larger in the solution of the GY equation.

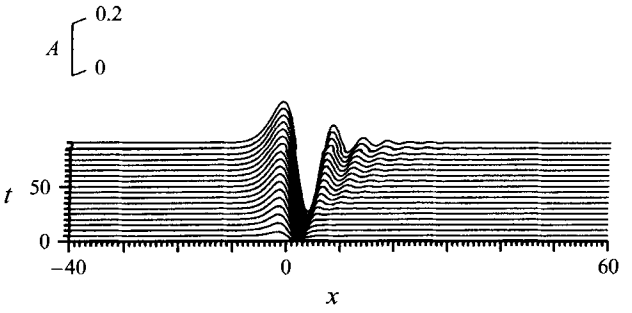

FIGURE 13. Time development of $A = A_1(x, t)$ obtained by the GY equation ($\epsilon = 0.01$) when the waves are excited by a large local contraction of the tube wall given by (17b) with $h = -0.015$ ($F = 1.0$). Note that in figures 13, 14(b), 17(b) and 19(b), the scale of A is twice that of the previous figures since the wave amplitude become large.

Comparing figure 12(a) with figure 10(c), and figure 12(b) with figure 11(c), we note that, for the same strength of the forcing $|g(X)|$ with opposite sign ($h = \pm 0.005$ in (17b)), the resultant wave amplitude $A(x, t)$ has approximately the same modulus and the opposite sign everywhere. This is because, in the forcing term of the GY equation (13b), $j_n^2 J_0(j_n) A/|2\Omega| \ll 1$ holds for sufficiently small $A(x, t)$. In the present case, the maximum value of $|A|$ is about 0.16 so that $j_n^2 J_0(j_n)|A|/|2\Omega| \approx 0.25$ for $n = 1$. Therefore, the GY equation (13b) is not susceptible to the simultaneous change of $g \to -g$ and $A \to -A$ as long as $|A|$ is not so large and $K(A, A') \approx 1$ holds so that the GY equation can be approximated by the fKdV equation with weak nonlinearity. Of course, as time proceeds and the modulus of the wave amplitude A becomes much larger, the similarity between figures 11(a) and 9(c), or figures 11(b) and 10(c), will become worse.

From the results for the nearly resonant conditions ($F \approx 1$), we can say that the GY equation describes well the nonlinear behaviour of the inertial waves excited by various forcings near resonance. Then, the remaining question is the possibility of predicting the onset of the axial flow reversal leading to the generation of the recirculation eddies. For this purpose, we use a local contraction of the tube wall. This type of excitation is chosen, since the violation of the lower limit of A in (16c) is easier than the violation of its upper limit, whose modulus is about 2.5 times larger. In addition, we saw, in the results described above, a wave of depression just downstream of the excited position has the largest modulus. Then, if its value is negative, we expect that the violation of the lower limit is most likely to occur. This is just the case of the local contraction of the tube wall that we have seen in figures 10 and 11. Here, we use a contraction whose radial amplitude is three times larger than that used in figures 9, 10 and 11 to generate the waves of larger amplitude which would lead to an axial flow reversal. As mentioned in §2.2, the violation of the lower limit of $A(x, t)$ causes the flow reversal on the tube axis ($r = 0$). This is in agreement with the vortex breakdown observed in laboratory experiments, although the rotation type is different. In a laboratory experiment for the vortex breakdown, local contraction of the tube wall was actually used by Kirkpatrick (1965) (see figure 6 of Hall 1972). In that experiment the vortex breakdown occurred where the tube radius was nearly minimum.

In figure 13 the solution of the GY equation is shown until the flow reversal occurs. The minimum of A occurs just downstream of the excited position and it reaches the lower limit of (16), i.e. $A(= -C_1/j_1 = -0.26)$ at $t = 92.45$ near $x = 4$, which would lead to the axial flow reversal on the tube axis. Therefore, further time development is

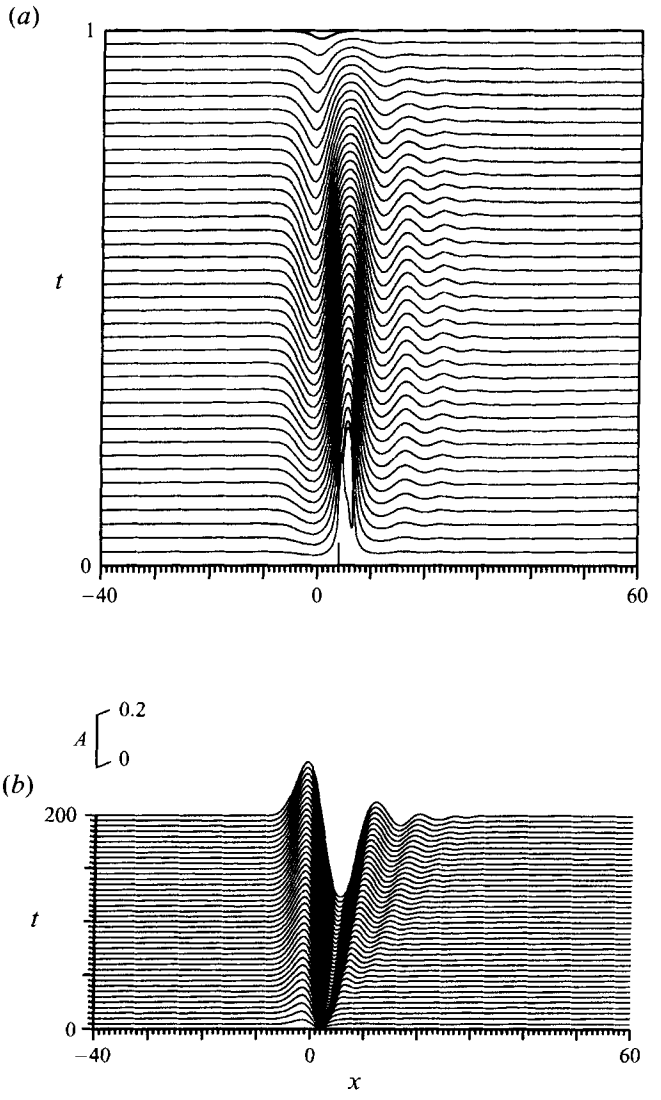

FIGURE 14. (*a*) Stokes streamlines at time $t = 200$ obtained from the solution of the Navier–Stokes equations when the waves are excited by a large local contraction of the tube wall given by (17*b*) with $h = -0.015$ ($Re = 10^5$, $F = 1.0$). Streamlines are drawn for $\psi = 3.125 \times 10^{-4} \times n^2$ ($0 \leqslant n \leqslant 40$). (*b*) Time development of $A = A_1(x, t)$ obtained from the solution of the Navier–Stokes equations.

impossible as discussed in §2.2. On the contrary, in the solution of the Navier–Stokes equations for $Re = 10^5$ (figure 14*b*), the minimum value of A decreases continuously until it reaches about -0.3 at $t = 200$. This is because, even when the axial flow reversal occurs, A can still be calculated by (20*b*). The comparison of figure 13 with figure 14(*b*), shows that the agreement between the solution of the Navier–Stokes equations and the GY equation is good until the lower limit of A is violated in the solution of the GY equation, except that the amplitude is somewhat larger in the solution of the GY equation. In the solution of the Navier–Stokes equations, axial flow reversal occurs at about $t = 140$. The onset time is later than the prediction of the Grimshaw–Yi equation because $|A|$ is smaller. The prediction of the onset time of the axial flow reversal is difficult, however, since the growing rate of the wave amplitude

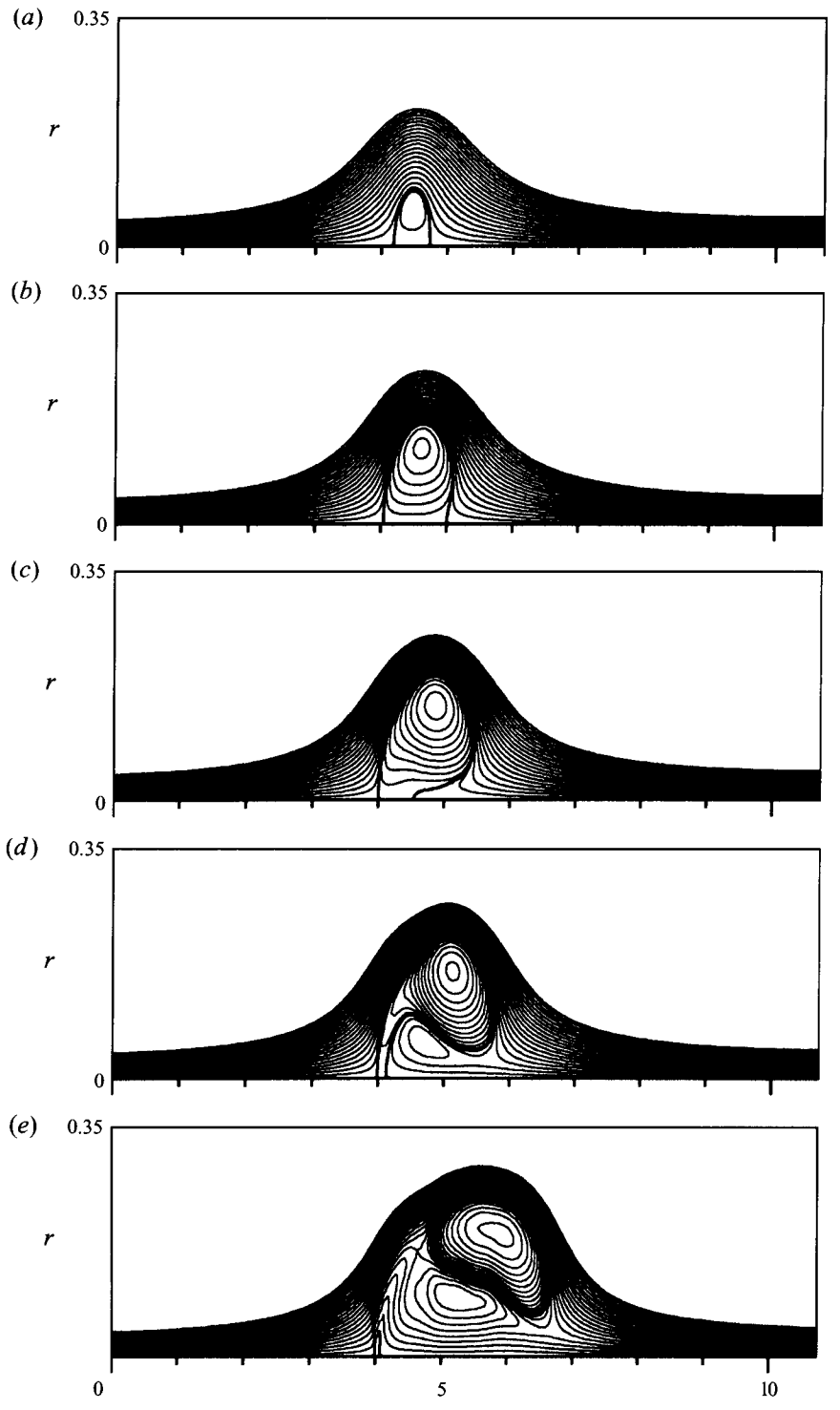

FIGURE 15. Time development of the Stokes streamlines in the recirculation eddies obtained from the solution of the Navier–Stokes equations when the waves are excited by a large local contraction of the tube wall given by (17*b*) with $h = -0.015$ ($Re = 10^5$, $F = 1.0$). Streamlines are drawn for $\psi = 3.125 \times 10^{-6} \times n^2$ ($0 \leqslant n \leqslant 20$): (*a*) $t = 140$; (*b*) $t = 150$; (*c*) $t = 160$; (*d*) $t = 170$; (*e*) $t = 200$.

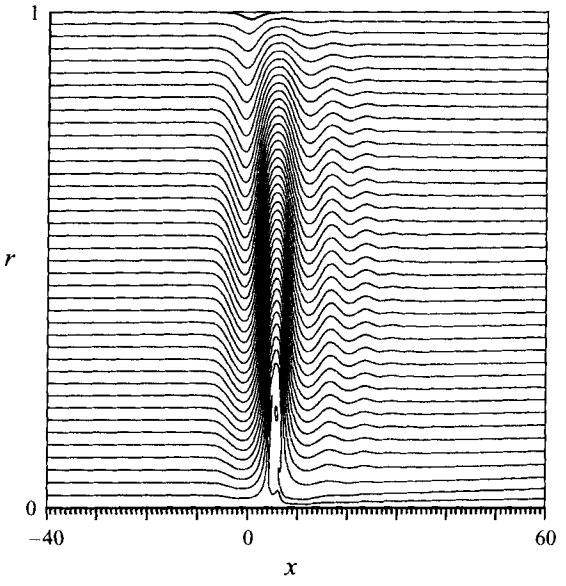

FIGURE 16. The contours of the circulation $\Gamma = rw$ at time $t = 200$ obtained from the solution of the Navier–Stokes equations when the waves are excited by a large local contraction of the tube wall given by (17*b*) with $h = -0.015$ ($Re = 10^5$, $F = 1.0$).

significantly decreases with time and a small difference in the amplitude leads to a rather large difference in the onset time of flow reversal (cf. §2.2). Therefore, we can say that the agreement is good.

To illustrate the typical flow patterns when the flow reversal occurred, streamlines at the final time of the computation is shown in figure 14(*a*). We see that an 'eddy' is formed under the largest wave ($0 \leqslant r \leqslant 0.3$ and $4 \leqslant x \leqslant 7$). Note here that the eddy is actually not narrow but long in the axial direction since the figure is reduced a 100 times in that direction. The onset position of the recirculation eddy ($x = 4.4$, cf. figure 15*a*) agrees well with the prediction by the GY equation.

To see the time development of the recirculation eddies, streamlines near the tube axis which are more enlarged in the axial direction are shown in figure 15. Initially, a small eddy is formed on the tube axis at $x = 4.4$. The first eddy becomes larger until the second eddy ($t \geqslant 170$) penetrates beneath the first eddy. We should note that once the reversed axial flow occurs, it develops into a large eddy in a much shorter time ($140 \leqslant t \leqslant 160$) than the time required for the onset of flow reversal. This qualitatively agrees with the laboratory experiments which reported a 'sudden' occurrence of the vortex breakdown. The flow in the breakdown bubble is highly unsteady. The unsteadiness could also be identified by the comparison of the contours of circulation ($\Gamma = rw$) with the Stokes streamlines as mentioned in §2. The contours of the circulation Γ which correspond to the streamlines shown in figure 14(*a*) are presented in figure 16. Outside the recirculation eddy, the unsteadiness is small and the contours of Γ and the streamlines coincide well, while in the recirculation region, they differ significantly owing mainly to the unsteadiness of the eddies.

We also note here that the pattern of the eddy structure given in figure 15(*d*), *e*($t = 170$, 200) is similar to the mean-streamline pattern obtained experimentally by Faler & Leibovich (1978) (see their figure 10). In their figure, a 'two-celled' structure is seen in the bubble interior and the outer cell is much stronger than the inner cell. These agree with the present results, although their experiments are carried out in a

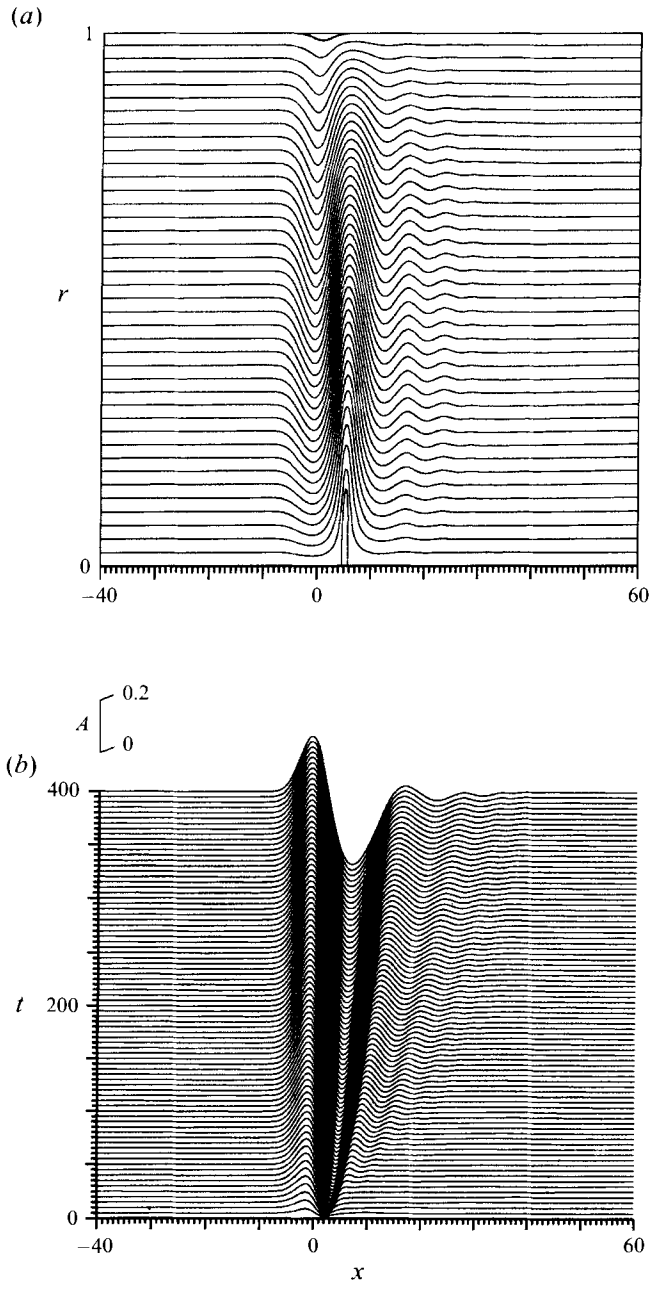

FIGURE 17. (*a*) Stokes streamlines at time $t = 200$ obtained from the solution of the Navier–Stokes equations when the waves are excited by a large local contraction of the tube wall given by (17*b*) with $h = -0.015$ ($Re = 10^4$, $F = 1.0$). Streamlines are drawn for $\psi = 3.125 \times 10^{-4} \times n^2$ ($0 \leqslant n \leqslant 40$). (*b*) Time development of $A = A_1(x, t)$ obtained from the solution of the Navier–Stokes equations.

monotonically diverging duct using a very different upstream velocity distribution (with a shear in the axial velocity and with a swirl of Burgers-vortex type). The resemblance suggests that the interior structure of the vortex breakdown is rather insensitive to the details of the upstream flow velocity distributions. We should also note that, although the vortex breakdown bubbles observed in the experiments are not

axisymmetric (Leibovich 1991), the flow may be nearly axisymmetric until the flow reversal occurs as observed in the experiments (Maxworthy, Hopfinger & Redekopp 1985), and the onset of the recirculation eddies would be predicted by the GY equation.

We note that the structures of the recirculation eddies were almost independent of the Reynolds number for higher Reynolds numbers. Even the inviscid simulation using the Euler equations gave similar eddy structures, although the results are not included here. Then, to investigate the effect of viscosity on the generation and the time development of the recirculation eddies, Navier–Stokes equations were solved for two much lower Reynolds numbers $Re = 10^4$ and 10^3. When $Re = 10^4$ (figures 17 and 18) the flow reversal occurs at $t = 175$ (figure 18*a*) and the recirculation eddy grows until $t \approx 250$ (figure 18*c*). However, it shrinks again until the end of the computation ($t = 400$, figure 18*e*). This suggests that $Re = 10^4$ is on the verge of the generation of recirculation eddies and at the same time this illustrates the subtleness of the phenomena. Figure 17(*b*) shows that, although the length of the first negative region of A ($0 \leqslant x \leqslant 10$) becomes longer with time, the minimum (negative) value of A stops a further decrease for $t \geqslant 200$ and remains constant ($A = -0.27$). This is the reason why the recirculation eddies were not strengthened any more.

It is important to note that the recirculation eddies, which are local phenomena, are largely determined by the global structure of the inertial wave and the very slight changes in the large-scale waves result in a large difference in the time development and the structure of the recirculation eddies. This illustrates the severe subtleness in the problem of the vortex breakdown, if the vortex breakdown observed in the experiments are essentially generated by the inertial waves.

Finally, the results for the case of $Re = 10^3$ are presented in figure 19. In this case the flow becomes completely 'steady' after $t \approx 200$ and the flow reversal does not occur because the wave amplitude A maintained a constant value. A similar steady solution has been obtained by Smyth (1988, see his figure 10*b*) in the solution of the fKdV–Burgers equation with a negative forcing which corresponds to the tube wall contraction in this study. In the case of the fKdV–Burgers equation, the amplitude stops time development if the viscosity is sufficiently large. Our results are for uniform rotation which are not described by the fKdV–Burgers equation. However, similar viscosity effects can be expected since the GY equation reduces to the fKdV equation in the weakly nonlinear limit (see §2.2). The recirculation eddies appear only when the Reynolds number is sufficiently large, although the lowest limit for the flow reversal depends on the strength of the excitation source and the Froude number. This qualitatively agrees with the laboratory experiments for the vortex breakdown where axisymmetric or 'bubble type' breakdowns were observed only at high Reynolds numbers (typically $Re > 10^3$).

5. Conclusions

We have investigated the fundamental linear and nonlinear aspects of the inertial waves excited by the topographic forcings. When the flow is subcritical, the excited waves have many linear aspects, including the speed of the upstream-advancing wave and the wavelength of the standing lee waves. The shortest wavelength components which can appear upstream of the obstacle were also identified. It was also confirmed that the second mode ($n = 2$) is not excited until that mode becomes near resonance.

We found that when the flow is near the critical (resonant) condition of the first mode ($n = 1$), the waves are dominated by the first mode and are described well by the Grimshaw–Yi equation for the first mode. The equation could describe the time

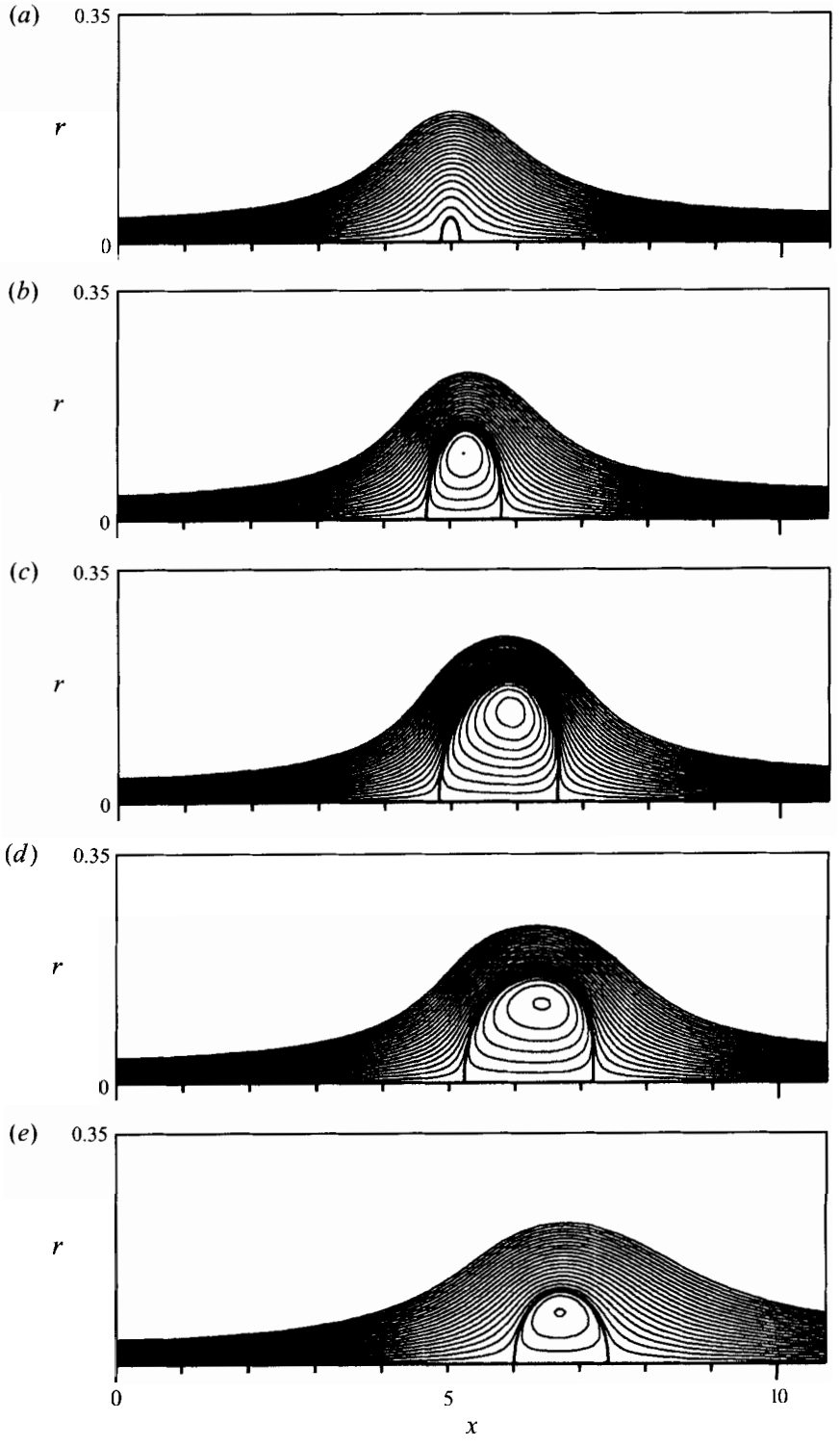

FIGURE 18. Time development of the Stokes streamlines in the recirculation eddies obtained from the solution of the Navier–Stokes equations when the waves are excited by a large local contraction of the tube wall given by (17*b*) with $h = -0.015$ ($Re = 10^4$, $F = 1.0$). Streamlines are drawn for $\psi = 3.125 \times 10^{-6} \times n^2$ ($0 \leqslant n \leqslant 20$): (*a*) $t = 175$; (*b*) $t = 200$; (*c*) $t = 250$; (*d*) $t = 300$; (*e*) $t = 400$.

development of the mode $n = 1$ wave irrespective of whether the waves are excited by the obstacle on the tube axis or by the local expansion/contraction of the tube wall. Even when the wave amplitude becomes large enough to cause flow reversal, the Grimshaw–Yi equation was found to be useful in many respects. It predicts the location of the breakdown accurately although the prediction of the exact time of its occurrence is difficult since the growth rate of the wave amplitude becomes much smaller as the wave amplitude approaches the limit value necessary for the onset of flow reversal. In this study, local contraction of the tube wall was used to investigate the generation and the time development of the recirculation eddies, since it was found in the course of this study that the violation of the wave-amplitude limit necessary for the axial flow reversal most easily occurs in this case. The unsteadiness in the recirculation region was found to be much larger compared to the flow around it.

The structures of the recirculation eddies are affected by the change of the Reynolds number if the Reynolds number is not very large ($Re \leqslant 10^5$). When the Reynolds number is small ($Re = 10^3$), the flow becomes steady without leading to a flow reversal, although the lowest limit Reynolds number for the generation of the recirculation eddies must depend on the Froude number and the strength of the excitation source, i.e. the size of an obstacle or a tube deformation.

The main purpose of this paper is in the investigation of the fundamental linear and nonlinear aspects of the waves excited in uniformly rotating flows and not in the precise reproduction of the vortex breakdown phenomena which have been observed in the previous experiments. However, if the essential aspects of the vortex breakdown are in the 'inertial waves', we can say that the essential mechanism of the vortex breakdown is included in this study. Only when the flow is near critical (resonant) conditions, are large-amplitude waves excited causing the flow reversal which forms the recirculation eddies. The structure of the recirculation eddies, i.e. the two-celled structure, was similar to the experiments although the upstream velocity distribution was different. It is necessary to study the case of non-uniform (e.g. Burgers-vortex type) rotation to investigate further the direct relation to the vortex breakdowns observed in experiments.

In a future numerical study of the vortex breakdown, precise reproduction of the phenomena using exactly the same conditions as the laboratory experiments is necessary, since most of the previous studies used a straight tube, which is different from the experiments. However, even if it were done, theoretical interpretation of the results would still be difficult for a 'diverging' tube, since the tube radius and the axial flow velocity changes along the flow and the construction of the wave theory becomes difficult (Faler & Leibovich 1978). The Grimshaw–Yi equation, of course, has limitations in its applicability conditions. For example, it can be applied only to the 'localized' topographic effects and not to the diverging tube. However, this is the only existing strongly nonlinear theory for the inertial wave, and this numerical study is an illustration of the 'wave' mechanism for the generation of the recirculation eddies, including the test of the applicability of the GY equation. The vortex breakdown may have its origin in the instability of the flow, and its possibility should be investigated separately. The investigation of each mechanism should be done before the precise numerical reproductions of the vortex breakdowns are done, so that the mechanisms of the phenomena become clear. The investigation of the non-axisymmetric effects using three-dimensional Navier–Stokes equations would also be important to investigate the time development of the recirculation eddies, since it is affected largely by the non-axisymmetric effects.

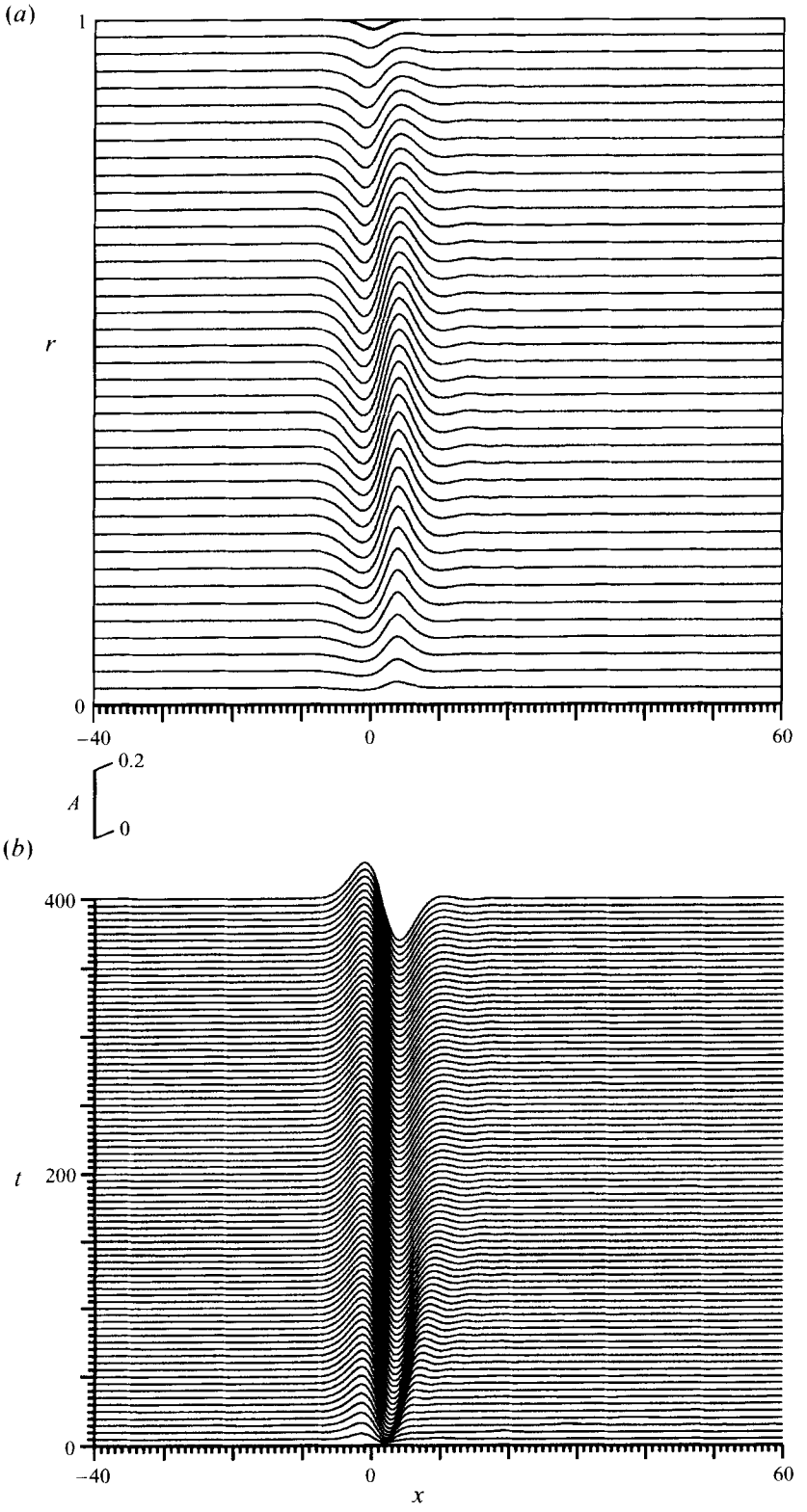

FIGURE 19. For caption see facing page.

I would like to thank Professor R. H. J. Grimshaw of Monash University for sending me the paper by Grimshaw & Yi (1993) before its publication, and also for his valuable comments on the results of my computation.

Appendix

We have used the MAC (marker and cell) method commonly used for the incompressible fluid flows. We use an upwind scheme of third-order accuracy for the nonlinear terms (Kawamura, Takami & Kuwahara 1986) and a central difference of second-order accuracy for all the other space derivatives. We use the body-fitted curvilinear coordinates (Thames *et al.* 1977) to accurately incorporate the effect of the boundary deformation.

The grid spacing is $\Delta x = 0.0625$ where $-5 < x < 5$, and becomes gradually larger where $|x| > 5$. To describe the boundary deformation accurately, the grid points are concentrated toward both the tube axis and the tube wall. The minimum grid spacing is about $\Delta r = 2.5 \times 10^{-3}$ (at $r = 0$ and $r = 1$) and becomes gradually large toward $r = 0.5$.

To be explicit, the grid is given by

$$x(I) = -5-(-5-x_{min})\frac{170-I}{170}\left(1-\tanh\frac{I}{170}\right)^{0.8} \qquad (0 \leqslant I \leqslant 170), \tag{A 1}$$

$$= -5+10\frac{I-170}{160} \qquad (170 \leqslant I \leqslant 330), \tag{A 2}$$

$$= 5+(x_{max}-5)\frac{I-330}{I_{max}-330}\left(1-\tanh\frac{I_{max}-I}{I_{max}-330}\right)^{0.7} \qquad (330 \leqslant I \leqslant I_{max}), \tag{A 3}$$

and

$$r(J) = r_{in}+(0.5-r_{in})\frac{2J}{J_{max}}\left(1-\tanh\frac{J_{max}-2J}{J_{max}}\right) \qquad \left(0 \leqslant J \leqslant \frac{J_{max}}{2}\right), \tag{A 4}$$

$$= r_{out}-(r_{out}-0.5)\frac{2(J_{max}-J)}{J_{max}}\left(1-\tanh\frac{2J-J_{max}}{J_{max}}\right) \qquad \left(\frac{J_{max}}{2} \leqslant J \leqslant J_{max}\right), \tag{A 5}$$

where

$$x_{min} = -40, \quad x_{max} = 60, \quad I_{max} = 650, \quad J_{max} = 100, \quad r_{in} = r(J = 0),$$
$$r_{out} = r(J = J_{max}).$$

For the time development, explicit Euler method of first-order accuracy was used. The value of Δt is $\Delta t = 0.002$ when there is no flow reversal and $\Delta t = 0.001$ when there is a flow reversal. This is because the unsteadiness is larger inside the recirculation eddies. Then the computation was done typically until $t = 200$. Then, the number of timesteps

FIGURE 19. (*a*) Stokes streamlines at time $t = 400$ obtained from the solution of the Navier–Stokes equations when the waves are excited by a large local contraction of the tube wall given by (17*b*) with $h = -0.015$ ($Re = 10^3$, $F = 1.0$). Streamlines are drawn for $\psi = 3.125 \times 10^{-4} \times n^2$ ($0 \leqslant n \leqslant 40$). (*b*) Time development of $A = A_1(x, t)$ obtained from the solution of the Navier–Stokes equations.

was typically 10^5. Typical CPU time for each calculation on NEC SX-3 (5GFlops on single processor) were 30 min if we use $\Delta t = 0.002$ and 1 h if we use $\Delta t = 0.001$.

The numerical accuracy was checked using the case of $Re = 10^5$, with the tube contraction given by (17*b*) ($h = -0.015$) since this case has the largest wave amplitude and then the strongest recirculation eddies are generated. In addition, this case has the largest Reynolds number in this study and the effect of the numerical errors should appear most seriously. It was found that the effect of the further reduction in Δx was completely negligible since the halving of the values of Δx given by (A 1)–(A 3), i.e. the use of $I_{max} = 1300$, gave no quantitative differences. The effect of halving the size of Δr, i.e. the use of $J_{max} = 200$, was also negligibly small. Note also that the number of radial grid points ($= 100$) are originally several times larger than the previous numerical studies for the vortex breakdown, in which typically 30 points were used. On the other hand, the effect of the reduction of Δt was a little problematic. The values used in this study ($\Delta t = 0.002$, 0.001) are much smaller than those used in the previous numerical studies for the unsteady vortex breakdown, where it was typically $\Delta t = 0.02$–0.04. However, the strength of the recirculation eddies still had some sensitivities to the further reduction of Δt. For example, the use of $\Delta t = 0.0005$ gave the strength of the recirculation eddies still weaker than that obtained with $\Delta t = 0.001$ presumably because the numerical viscosity has been reduced and the numerical vorticity generation was reduced. However, the patterns of the eddy structure were unchanged so we can say the results given in figure 15 are reliable at least in the 'fundamental' eddy structure. We should also note that the wave amplitude A_1 was altered only slightly by the reduction of Δt. Then, except for the strength of the recirculation eddy (if it exists), the reduction of Δt does not give meaningful changes to the results. The use of the Crank–Nicholson method, which has second-order accuracy in time, did not change the results quantitatively, showing that this is a rather subtle problem of numerical errors which cannot be implemented by simply using the higher-order time-integration scheme.

REFERENCES

Akylas, T. R. 1984 On the excitation of long nonlinear waves by a moving pressure distribution. *J. Fluid Mech.* **141**, 455–466.

Baines, P. G. 1979 Observations of stratified flow over two-dimensional obstacles in fluid of finite depth. *Tellus* **31**, 351–371.

Batchelor, G. K. 1967 *An Introduction to Fluid Dynamics*. Cambridge University Press.

Benjamin, T. B. 1962 Theory of the vortex breakdown phenomenon. *J. Fluid Mech.* **14**, 593–629.

Benjamin, T. B. 1967 Some developments in the theory of the vortex breakdown. *J. Fluid Mech.* **28**, 65–84.

Benjamin, T. B. 1970 Upstream influence. *J. Fluid Mech.* **40**, 49–79.

Benny, D. J. 1979 Large amplitude Rossby waves. *Stud. Appl. Maths* **60**, 1–10.

Beran, P. S. 1987 Numerical simulations of trailing vortex bursting. *AIAA Paper* 87–1313.

Beran, P. S. & Culick, F. E. 1992 The role of non-uniqueness in the development of vortex breakdown in tubes. *J. Fluid Mech.* **242**, 491–527.

Castro, I. P. & Snyder, W. H. 1988 Upstream motions in stratified flow. *J. Fluid Mech.* **187**, 487–506.

Faler, J. H. & Leibovich, S. 1977 Disrupted states of vortex flow and vortex breakdown. *Phys. Fluids* **20**, 1385–1400.

Faler, J. H. & Leibovich, S. 1978 An experimental map of the internal structure of a vortex breakdown. *J. Fluid Mech.* **86**, 313–335.

Grabowski, W. J. & Berger, S. A. 1976 Solutions of the Navier–Stokes equations for vortex breakdown. *J. Fluid Mech.* **75**, 525–544.

GRIMSHAW, R. 1990 Resonant flow of rotating fluid past an obstacle: The general case. *Stud. Appl. Maths* **83**, 249–269.

GRIMSHAW, R. H. J. & SMYTH, N. 1986 Resonant flow of a stratified fluid over topography. *J. Fluid Mech.* **169**, 429–464.

GRIMSHAW, R. & YI, Z. 1991 Resonant generation of finite-amplitude waves by the flow of a uniformly stratified fluid over topography. *J. Fluid Mech.* **229**, 603–628.

GRIMSHAW, R. & YI, Z. 1993 Resonant generation of finite-amplitude waves by the uniform flow of a uniformly rotating fluid past an obstacle. *Mathematika*, **40**, 30–50.

HAFEZ, M., AHMAD, J., KURUVILA, G. & SALAS, M. D. 1987 Vortex breakdown simulation. *AIAA paper* 87–1343.

HAFEZ, M., KURUVILA, G. & SALAS, M. D. 1986 Numerical study of vortex breakdown. *AIAA paper* 86–0558.

HALL, M. G. 1972 Vortex breakdown. *Ann. Rev. Fluid Mech.* **4**, 195–218.

HANAZAKI, H. 1989 Upstream advancing columnar disturbances in two-dimensional stratified flow of finite depth. *Phys. Fluids* A **1**, 1976–1987.

HANAZAKI, H. 1991 Upstream-advancing nonlinear waves in an axisymmetric resonant flow of rotating fluid past an obstacle. *Phys. Fluids* A **3**, 3117–3120.

HANAZAKI, H. 1992 A numerical study of nonlinear waves in a transcritical flow of stratified fluid past an obstacle. *Phys. Fluids* A **4**, 2230–2243.

HANAZAKI, H. 1993*a* Upstream-advancing nonlinear waves excited in an axisymmetric transcritical flow of rotating fluid. *Phys. Fluids* A **5**, 568–577.

HANAZAKI, H. 1993*b* On the nonlinear internal waves excited in the flow of a linearly stratified Boussinesq fluid. *Phys. Fluids* A **5**, 1201–1205.

HARVEY, J. K. 1962 Some observations of the vortex breakdown phenomenon. *J. Fluid Mech.* **14**, 585–592.

KAWAMURA, T., TAKAMI, H. & KUWAHARA, K. 1986 Computation of high Reynolds number flow around a circular cylinder with surface roughness. *Fluid Dyn. Res.* **1**, 145–162.

KIRKPATRICK, D. L. I. 1965 Experimental investigation of the breakdown of a vortex in a tube. *Aeronaut. Res. Counc. CP* no. 821.

KOPECKY, R. M. & TORRANCE, K. E. 1973 Initiation and structure of axisymmetric eddies in a rotating stream. *Comput. Fluids* **1**, 289–300.

LEE, S. J., YATES, G. T. & WU, T. Y. 1989 Experiments and analyses of upstream-advancing solitary waves generated by moving disturbances. *J. Fluid Mech.* **199**, 569–593.

LEIBOVICH, S. 1969 Evolution of nonlinear waves in rotating fluids. *Phys. Fluids* **12**, 1124–1126.

LEIBOVICH, S. 1970 Weakly nonlinear waves in rotating fluids. *J. Fluid Mech.* **42**, 803–822.

LEIBOVICH, S. 1978 The structure of vortex breakdown. *Ann. Rev. Fluid Mech.* **10**, 221–246.

LEIBOVICH, S. 1983 Vortex stability and breakdown: survey and extension. *AIAA J.* **22**, 1192–1206.

LEIBOVICH, S. 1991 Vortex breakdown: a coherent transition trigger in concentrated vortices. In *Turbulence and Coherent Structures* (ed. O. Metais & M. Lesieur). Kluwer.

LEIBOVICH, S. & RANDALL, J. D. 1973 Amplification and decay of long nonlinear waves. *J. Fluid Mech.* **53**, 481–493.

LONG, R. R. 1953 Steady motion around a symmetrical obstacle moving along the axis of a rotating liquid. *J. Met.* **10**, 197–203.

MCINTYRE, M. E. 1972 On Long's hypothesis of no upstream influence in uniformly stratified or rotating fluid. *J. Fluid Mech.* **52**, 209–243.

MAXWORTHY, T., HOPFINGER, E. J. & REDEKOPP, K. G. 1985 Wave motions on vortex cores. *J. Fluid Mech.* **151**, 141–165.

MELVILLE, W. K. & HELFRICH, K. R. 1987 Transcritical two-layer flow over topography. *J. Fluid Mech.* **178**, 31–52.

MENNE, S. 1988 Vortex breakdown in an axisymmetric flow. *AIAA Paper* 88-0506.

PRITCHARD, W. G. 1968 A study of wave motions in rotating fluids. PhD dissertation, University of Cambridge.

PRITCHARD, W. G. 1969 The motion generated by a body moving along the axis of a uniformly rotating fluid. *J. Fluid Mech.* **39**, 443–464.

RANDALL, J. D. & LEIBOVICH, S. 1973 The critical state: A trapped wave model of vortex breakdown. *J. Fluid Mech.* **53**, 495–515.

ROTTMAN, J. W., BROUTMAN, D. & GRIMSHAW, R. 1996 Numerical simulations of the flow of a uniformly stratified, inviscid Boussinesq fluid over long topography in a channel of finite depth. *J. Fluid Mech.* **306**, 1–30.

SALAS, M. D. & KURUVILA, G. 1989 Vortex breakdown simulation: a circumspect study of the steady, laminar, axisymmetric model. *Comput. Fluids* **17**, 247–262.

SARPKAYA, T. 1971 On stationary and travelling vortex breakdowns. *J. Fluid Mech.* **45**, 545–559.

SMYTH, N. F. 1988 Dissipative effects on the resonant flow of a stratified fluid over topography. *J. Fluid Mech.* **192**, 287–312.

TAYLOR, G. I. 1922 The motion of a sphere in a rotating liquid. *Proc. R. Soc. Lond.* A **102**, 180–189.

THAMES, F. C., THOMPSON, J. F., MASTIN, C. W. & WALKER, R. L. 1977 Numerical solutions for viscous and potential flow about arbitrary two-dimensional bodies using body-fitted coordinate systems. *J. Comput. Phys.* **24**, 245–273.

WU, T. Y. 1981 Long waves in ocean and coastal waters. *J. Engng Mech. Div. ASCE* **107**, 501–522.

YI, Z. & WARN, T. 1987 A numerical method for solving the evolution equation of solitary Rossby waves on a weak shear. *Adv. Atmos. Sci.* **4**, 43–54.